

Simulation-Based Inference for Parameter Estimation of Complex Watershed Simulators

Robert Hull¹, Elena Leonarduzzi², Luis De La Fuente¹, Hoang Viet Tran^{3,4}, Andrew Bennett¹, Peter Melchior^{5,6}, Reed M. Maxwell^{2,3,7}, Laura E. Condon¹

5 ¹ Hydrology and Atmospheric Sciences, University of Arizona, Tucson, AZ, USA

² High Meadows Environmental Institute, Princeton University, Princeton, NJ, USA

³ Civil & Environmental Engineering, Princeton University, Princeton, NJ, USA

⁴ Atmospheric Sciences & Global Change Division, Pacific Northwest National Laboratory, Richland, WA, USA

10 ⁵ Center for Statistics and Machine Learning, Princeton University, Princeton, NJ, USA

⁶ Department of Astrophysical Sciences, Princeton University, Princeton, NJ, USA

⁷ Integrated GroundWater Modeling Center, Princeton University, Princeton, NJ, USA

Correspondence to: Robert Hull (roberthull@email.arizona.edu)

15 **Abstract.** High-resolution, spatially distributed process-based (PB) simulators are widely employed in the study of complex catchment processes and their responses to a changing climate. However, calibrating these PB simulators to observed data remains a significant challenge due to several persistent issues including: (1) intractability stemming from the computational demands and complex responses of simulators, which renders infeasible calculation of the conditional probability of parameters and data, and (2) uncertainty stemming from the choice of simplified representations of complex natural hydrologic processes. Here we demonstrate how Simulation-Based Inference (SBI) can help address both these challenges for parameter estimation. SBI uses a learned mapping between parameter space and observed data to estimate parameters for generation of calibrated simulations. To demonstrate the potential of SBI in hydrologic modelling, we conduct a set of synthetic experiments to infer two common physical parameters, Manning's coefficient and hydraulic conductivity, using a representation of a 20 snowmelt-dominated catchment in Colorado, USA. We introduce novel deep learning (DL) components to the SBI approach, including an 'emulator' as a surrogate for the process-based simulator to rapidly explore parameter responses. We also employ a density-based neural network to represent the joint probability of parameters and data without strong assumptions about its 25 functional form. While addressing intractability, we also show that where the simulator does not represent the system under study well enough, SBI can yield unreliable parameter estimates. Approaches to adopting the SBI framework to cases multiple 30 simulator(s) may be adequate are introduced using a performance-weighting approach. The synthetic experiments presented here test the performance of SBI, using the relationship between the surrogate and PB simulators as a proxy for the real case.

1 Introduction

35 Robust hydrologic tools are necessary to understand and predict watershed (catchment) behaviors in a changing climate (Condon, 2022). This need is underscored by long-term drought in the American West (Williams et al., 2022), which

has led to the withering of water supplies from the Colorado River (Santos and Patno, 2022), increased groundwater pumping (Castle et al., 2014), and uncertainty about what is next (Tenney, 2022). Hydrologic simulators that represent physical processes and connections within the hydrologic cycle (Paniconi and Putti, 2015) are very commonly used tools to address these needs. These 'process-based' (PB) simulators explicitly represent hydrologic states and fluxes at multiple scales based 40 upon physics first-principles (Fatichi et al., 2016). Catchment scientists often use PB simulators to answer 'what if' questions about behavior of catchment snowpack, soil moisture, and streamflow in a changed future because they encode fundamental processes, and not just historical data (Maxwell et al., 2021).

The behaviors and skills of these PB catchment simulators (henceforth referred to as PB simulators) strongly depend on spatially varying parameters (Tsai et al., 2021). Parameters represent the structure and physical properties of the hydrologic 45 system, such as the roughness of the land surface (i.e., Manning's Coefficient, M) or the water-transmitting properties of the subsurface (i.e., Hydraulic Conductivity, K). There are many approaches to parameter determination in hydrology (Beven and Binley, 1992.; Gupta et al., 1998; Bastidas et al., 1999; Hunt et al., 2007; Vrugt and Sadegh, 2013; White et al., 2020; Tsai et al., 2021). The variety of approaches and long history of research in this area underscores that there is "no obvious formulation 50 of [parameter determination] that previous generations of modelers have overlooked" (Hunt et al., 2007). Yet, the question of how best to infer parameters for PB simulators remains unsettled.

Parameter determination remains a challenge with catchment PB simulators, and an impediment to robust, physics-informed hydrologic predictions. There are two related and ongoing difficulties that make parameter determination a very 55 challenging problem. The first is the problem of intractability. For a dynamical catchment simulator with a range of possible configurations, many combinations of parameters may be plausible given observed data (Beven, 2011; Nearing et al, 2015). Therefore, many have argued it may be preferable to simulate distributions of hydrologic variables and the underlying 60 parameters that give rise to them (e.g. Vrugt and Sadegh, 2013). Intractability arises when these distributions cannot be approximated for theoretical or computational reasons. For example, large-scale, high-resolution PB simulations can require massively parallel, high-performance computing (e.g., Maxwell et al., 2015), limiting the number of exploratory simulations due to computational demands. A solution to the problem of intractability needs to efficiently approximate complex distributions of probable parameters given observations with a sufficient level of accuracy and precision.

Deep learning (DL) may provide new opportunities vis-à-vis the intractability problem in parameter determination. In DL, behaviors are learned from data, as opposed to PB approaches, which derive behavior from established theory. The Earth Sciences have recently seen greater adoption of DL approaches (Wilkinson et al., 2016), for example in streamflow prediction (Kratzert et al., 2018). However, DL methods are not widely used in the prediction of distributed catchment 65 variables due to the "inadequacy of available data in representing the complex spaces of hypotheses" (Karpatne et al., 2017), such as catchment observations. Recently, there has been a push for methods that can incorporate process understanding into DL approaches (e.g., Zhao et al., 2019; Jiang et al., 2020). Still, studies are rare that employ DL to improve PB simulator

70 performance by aiding in the hunt for better parameters¹. Tsai et al. (2021) use a neural network to learn the mapping between observable attributes and unobserved physical parameters, for a set of catchment rainfall-runoff simulators optimized to a regional loss function. This ‘differentiable learning’ approach can effectively find parameter sets that yield continuity across neighbouring domains. While the approach is strong for spatial generalization of lumped catchment simulators, it does not explicitly address the case where many parameter sets may be plausible (the equifinality problem), nor does it provide a mechanism to constrain the role of deficiencies in the simulator on parameter estimates.

75 Simulation-based inference (SBI) is a DL-informed approach to PB parameter determination that has shown promise in particle physics (Cranmer et al., 2020), cosmology (Alsing et al., 2019), and neural dynamics (Lueckmann et al., 2017). In SBI, a neural network is employed to approximate the conditional density of parameters and simulated outputs from the behavior of a simulator. The learned conditional relationship can then be evaluated using observations to estimate a set of probable parameters. Surrogate simulators are neural networks that emulate the complex interdependence of variables, inputs, and parameters encoded in PB simulators, such as catchment simulators (Maxwell et al., 2021; Tran et al., 2021). Once trained, 80 surrogate simulators can closely mimic the PB simulator, run at a fraction of the cost, and speed up the exploration of parameter space. Restated, this approach uses one neural network (the ‘surrogate’) to quickly generate thousands of simulations that are utilized to train another neural network (via conditional density estimation) to develop a statistical representation of the relationship between parameters and simulated data. Via SBI, this statistical representation can be used to infer distributions of PB parameter values based on observed data. Assuming the model is correctly specified, the inferred set of parameters 85 accurately and precisely reflects the uncertainty of the parameter estimate (Cranmer et al., 2020). To our knowledge, applications of SBI in hydrology have been limited (e.g., Maxwell et al., 2021). A brief introduction to SBI is presented in the background section.

90 A second challenge to parameter determination is the problem of epistemic uncertainty arising from limited knowledge, data, and understanding of complex hydrologic processes. The sources of epistemic uncertainty in the modelling process are various, including: uncertainties in data (for example, in simulator inputs and misleading information in observed data used to train and assess simulators); uncertainties derived from performance measures and information to omit; and uncertainty about what the structure of the simulator should be, which arises from the inherent challenge of choosing simplified representations of complex processes (Leamer, 1978; Beven & Binley, 1992; Draper, 1995; Gupta et al., 2012; Nearing et al., 2015). For example, the structure of PB catchment simulators is defined by the mathematical description of hydrologic flows, 95 state variables, and parameters. This description may or may not be able to represent catchment behaviour without error. DL surrogate simulators trained to mimic PB behaviour inherit this assumed structure, in addition to error from imperfect training. In other words, uncertainty about structure arises from both the relationship between the PB simulator and the catchment under study, and the relationship between the surrogate and the PB simulators. In this work, we focus on a subclass of epistemic

¹ We make a distinction between the parameters of PB simulators and the parameters embedded in neural networks, which are optimized during training by backpropagation. In this report, we almost-exclusively refer to the parameters of PB simulators even as we discuss the capacity of neural networks to learn and represent them.

uncertainty of the appropriate simulator (both PB and surrogate) structure(s) known as “misspecification”, in which a unique
100 and optimal description of the catchment is assumed to exist but is unknown. Discounting the role of uncertainty about the appropriate simulator structure can have profound consequences on the insights we draw from inference tasks like parameter determination.

A common challenge is the potential under-representation of uncertainty stemming from the choice of simulator structure. This issue becomes evident when inference yields parameter estimates that are overly confident, which can be
105 problematic when a more conservative estimate that accounts for the inherent uncertainties about simulator structure is preferred (Beven, 2011; Cranmer, 2020; Hermans, 2021). One potential remedy is to perform inference using multiple simulators, with different underlying structures and quality of fit. Once a set of competing simulator structures is assembled, the challenge then becomes deciding how to combine them. Generalized Likelihood Uncertainty Estimation, or GLUE (Beven and Binley, 1992; Beven and Binley, 2014), associates a measure of belief with each selected simulator structure and parameter
110 configuration, forming a conceptually simple way of weighting ensembles of predictions to estimate uncertainty stemming from various sources. A similar principle underlies Bayesian Model Averaging, or BMA (Leamer, 1978; Hoeting et al, 1999; Raftery et al., 2005; Duan et al., 2007). While GLUE and BMA differ in their implementations, they both adhere to the principle that simulator structures capable of generating simulation results closely aligned with observations should hold stronger credibility and carry greater significance within an ensemble; and simulator structures less capable of producing behavioural
115 simulations should be assigned a low probability or rejected. In the case of GLUE, this measure of credibility is derived from a modeler’s choice of metric, or informal likelihood function (e.g. Smith et al, 2008). GLUE and BMA are further described in the background section.

The primary objective of this work is to demonstrate an approach to generating accurate and precise estimates of the spatially distributed parameters of a PB hydrologic simulator where conventional methods might struggle due to the
120 intractability problem. A secondary goal is to explore how this workflow could be extended to yield meaningful parameter estimates considering uncertainty about the appropriate simulator (surrogate or PB) structure. Surrogate-derived SBI is utilized to address the problem of intractability in complex parameter spaces using a statistical, deep-learning approach. The problem of simulator misspecification is confronted using a quasi-BMA approach that utilizes an informal likelihood to weight the credibility of parameter estimates from SBI.

We use synthetic test cases with diagnosable degrees of error to test the performance of the inference workflow. Here, we determine the physical parameters of a headwater subcatchment of the Upper Colorado River Basin by calibrating a PB simulator to streamflow observations. We utilize SBI in tandem with a Long Short-Term Memory (LSTM) surrogate (henceforth referred to as the surrogate simulator) for the PB simulator ParFlow (Jones and Woodward, 2001; Maxwell and Kollet, 2006; Maxwell et al., 2015a) to rapidly generate probable configurations of Hydraulic Conductivity (K) and Manning’s
130 Coefficient (M). Furthermore, we use the inferred distribution of parameters to generate streamflow predictions. The experiments presented use the relationship between the surrogate and PB simulators as a proxy for the real case. We explore the influence of synthetic observations on parameter inference with a set of experiments that systematically vary the degree of

error in the simulator (i.e., misspecification). In the latter experiments, a form of BMA is utilized to improve robustness of the parameter estimates to misspecification, in the extreme case by assigning zero probability to all models in the set. The 135 experiments are outlined in Section 3.1.

Novel aspects of the present analysis that bear noting include: (1) the usage of DL in conjunction with a PB catchment simulator to improve its performance; (2) the novel application of density-based SBI to the scientific domain of hydrology; and (3) the usage of informal likelihood measures to directly assign model probabilities to parameter estimates made by SBI in a manner similar to BMA. The significance of this work is to develop a framework to tackle harder inference problems in 140 catchment modeling, and other domains of the Earth Sciences where complex PB simulators are used.

2 Background of inference-based approaches to hydrologic parameter determination

This section provides a brief background of methods used for parameter determination in catchment simulation. We provide context relevant to understanding the “point of convergence” (Cranmer et al., 2020) we call simulation-based inference (SBI), and how it is similar to and different from some other approaches to inference. We start with a general overview of 145 inference. Next, we discuss the traditional formulation of the inference of parameters using Bayes’ theorem (section 2.1). We then introduce what sets SBI apart from these traditional approaches (section 2.2). Next, we discuss the role of machine learning in SBI (section 2.3). Finally, we introduce some approaches to parameter estimation under epistemic uncertainty that have been applied in hydrology (2.4). For this section, ‘simulator’ generically refers to a computer program that requires some 150 number of parameters and produces output data; this term encompasses most PB simulators, and their surrogates, used in hydrology and other research domains. The term ‘model’ refers to the statistical relationship between parameters and outputs, which is defined implicitly by a simulator (PB or surrogate). We define ‘inference’ as using observations (data) and the statistical model defined by a simulator to describe unobserved characteristics (parameters) of the system we are interested in (Cranmer et al., 2020; Wikle and Berliner 2007).

2.1 Bayesian inference

155 Bayesian inference is a common method to extract information from observations. The essence of this formulation of inference unfolds in three steps (Wikle and Berliner, 2007): (1) Formulate a ‘full probability model’, which emerges from the joint probability distribution of observable and unobservable parameters; (2) Infer the conditional distribution of the parameters given observed data; (3) Evaluate the fit of the simulator (given parameters inferred in step 2) and its ability to adequately characterize the process(es) of interest.

160 Traditionally, to tackle inference problems we apply Bayes’ Theorem. For illustration, let θ denote unobserved parameters of interest (such as Hydraulic Conductivity); and let Y represent simulated or observed data of the variable of interest (such as streamflow). The joint probability $p(\theta, Y)$ can be factored into the conditional and marginal distribution by applying Bayes’ Rule, such that we obtain:

$$p(\theta|Y) = \frac{p(Y|\theta) p(\theta)}{p(Y)} \quad (1)$$

165 Where,

- The *data distribution*, $p(Y|\theta)$, is the distribution of data given unobservable parameters. This distribution is referred to as the likelihood when viewed as a function of θ for a fixed Y . The likelihood function of “implicit” simulators (such as those used in catchment hydrology) is often regarded as ‘intractable’ – i.e., its form cannot be evaluated (integrated), at least not in a computationally-feasible way (Cranmer et al., 2020).
- The *prior distribution*, $p(\theta)$, is our *a priori* understanding of unobservable parameters. The prior often results from a choice made by the domain expert. For example, in catchment simulation the prior distribution arises from a belief about the possible structures and magnitudes of parameters (for example, hydraulic conductivity) in a study domain, as well as the probability that they could be observed.
- The *marginal distribution*, $p(Y)$, can be thought of as a normalizing constant or ‘evidence’. In practice, this distribution is rarely computed as it contains no information about the parameters. As such, we do not include $P(Y)$ and instead work with the unnormalized density provided by Equation 2:

$$p(\theta|Y) \propto p(Y|\theta) p(\theta) \quad (2)$$

- The *posterior distribution*, $p(\theta|Y)$, which is the distribution of unobservable parameters given the data. The posterior is the primary goal of Bayesian inference; it is proportional to the product of our prior knowledge of parameters and the information provided in our observations.

180 Inference conducted using a Bayesian paradigm has a long history in computational hydrology (Vrugt and Sadegh, 2013). However, applications have been somewhat limited due to challenges centering on the intractability of the data distribution, $p(Y|\theta)$, for catchment simulators with many parameters.

2.2 Simulation-based inference

185 SBI is a set of methods that attempt to overcome the intractability of the data distribution by learning the form of the posterior distribution directly from the behavior of the simulator itself (Tejero-Cantero et al., 2020). There are a range of SBI approaches, some of which include deep learning, but traditionally deep learning has not been part of SBI workflows. The classic approach is Approximate Bayesian Computation (ABC), which compares observed and simulated data, rejecting and accepting simulation results based on some distance measure (Fenicia et al., 2018; Vrugt and Sadegh, 2013; Weiss and von 190 Haeseler, 1998). While this approach has been widely used, it suffers from a range of issues, including poor scaling to high-dimensional problems (resulting in the need for summary statistics), and uncertainty arising from the selection of a distance threshold (Alsing et al., 2019). Additionally, in traditional ABC it is necessary to restart the inference process as new data become available (Papamakarios and Murray, 2016), making it inefficient to evaluate large numbers of observations (Cranmer et al., 2020).

SBI methods predicated on density estimation enable an alternative that does not suffer from the same shortcomings of ABC. The density estimation approach aims to train a flexible density estimator of the posterior parameter distribution from a set of simulated data-parameter pairs (Alsing et al., 2019). Some of the key advantages of a density estimation approach over ABC: (a) it represents the posterior² distribution parametrically (as a trained neural network) that can be reused to evaluate new data as it comes available; (b) it drops the need for a distance threshold by targeting an ‘exact’ approximation of the posterior; (c) it more efficiently uses simulations by adaptively focusing on the plausible parameter region (Papamakarios and Murray, 2016).

One general purpose workflow that we employ in this paper uses a neural density estimator to learn the distribution of streamflow data as a function of the physical parameters of the simulator and employs active learning algorithms to run simulations in the most relevant regions of parameter space (Alsing et al., 2019; Lueckmann et al., 2017). The SBI workflow 205 is further described in Sect. 3.5, and the neural density estimator is described in Sect. 3.6.

2.3 The role of Machine Learning in SBI

Due to advances in the capacity of neural networks to learn complex relationships, we can learn high-dimensional probability distributions from data in a way that was hardly possible before (Cranmer et al., 2020). This has led to strong claims 210 in other fields, including cosmology and computational neuroscience, regarding the potential of SBI to “shift the way observational [science] is done in practice” (Alsing et al., 2019). While our implementation is described in more detail throughout the methods section, we direct readers to the literature for a broader (Cranmer et al., 2020) and deeper (Papamakarios and Murray, 2016) understanding of density based SBI.

Learning the full conditional density $p(\theta|Y)$ requires many simulated parameter-data pairs: thousands (or hundreds of thousands) of forward simulations. This presents a challenge with some high-resolution PB simulators, where each forward 215 simulation can take hours of computer time to run. Many have noted that deep-learned surrogate simulators can help; after an initial simulation and training phase, these simulators can be run forward very efficiently. “Surrogate-derived approaches benefit from imposing suitable inductive bias for a given problem” (Cranmer et al., 2020). In our case, this “inductive bias” is applied by learning the rainfall-runoff response of our PB domain using a Long Short-Term Memory (LSTM) simulator, a type of neural network that is suited for learning temporal patterns in data (Kratzert et al., 2018). The surrogate simulator is 220 described in more detail in Sect. 3.3. Surrogate simulators can be used directly in the construction of viable posterior distributions of physical parameters and run at low-cost relative to the PB simulator.

It should be noted that inference is always done within the context of a simulator (Cranmer, 2022). As such, if the simulator structure is not adequate, it will affect inference in undesirable ways. Simulator structural inadequacy arises in the case when a simulator does not capture the behavior of the dynamical system, giving rise to mismatch between simulated and

² We share the literature’s tendency to use ‘conditional’ and ‘posterior’ density interchangeably; denotations of $p(\theta | Y = Y_{True})$, for the posterior density evaluated at an observation Y_{Obs} ; and $p(\theta | Y)$, for conditional density representative of a large set of simulated $\{\theta, Y\}$, are used when possible to reduce ambiguity.

225 observed data (Cranmer et al., 2020). SBI conducted with structurally inadequate simulators can result in overly precise and otherwise erroneous inference. Similar concerns about the quality of inference arise from other potential sources of epistemic uncertainty in the modeling process, such as undiagnosed error in the data used to condition the model.

2.4 Model combination and parameter determination in hydrology

230 As simulator structural adequacy is not guaranteed, basing inference on one simulator structure alone is risky (Hoeting et al, 1999). Bayesian Model Averaging (BMA) is an approach developed in the statistical literature (Madigan and Raftery, 1994) to address this problem. BMA creates an updated statistical model by combining two or more competing ones (Roberts, 1965); in the case of dynamical systems, the competing models are defined implicitly by simulators with differing underlying structures. For example, BMA has been adopted to create weighted averages of climate forecasts derived from multiple simulators, each with different quality of fit to observed data (i.e. Raftery et al, 2005). Similarly, BMA has been used to 235 generate streamflow forecasts taken from several structurally distinct rainfall-runoff simulators (Duan et al, 2006). Results from these analyses show that the weighted combination yields more accurate inference and descriptions of uncertainty than those derived from any one simulator.

240 BMA is introduced here generically and extended to the current analysis at the end of the section. Consider Y_{obs} to be observed data, such as a streamflow time series; a quantity of interest Δ to be inferred, such as a prediction or underlying set of parameters θ ; and the set of competing models M_1, \dots, M_K . Each model M_k is defined by a simulator with unique underlying structure, which encodes the simulated data Y for possible values of θ . The probability of Δ in the presence of Y_{obs} can be represented as a weighted average, such that:

$$p(\Delta | Y_{obs}) = \sum_{k=1}^K p(\Delta | M_k, Y_{obs}) w_k \quad (3)$$

Where:

245

- $p(\Delta | M_k, Y_{obs})$ is the posterior distribution of Δ given the model under consideration M_k and Y_{obs} , which can be interpreted as the conditional probability of Δ given that M_k is the best model in the set (Raftery et al, 2005), and
- w_k is the posterior model probability, or the model weight. This can be interpreted as the posterior probability that model M_k is the best one (Raftery et al, 2005)

250 Even in relatively simple test cases (i.e. Raftery et al., 1997), the calculation of $p(\Delta | Y_{obs})$ is difficult due to the large number of possible models and computational and conceptual challenges related to w_k , and so defensible approximation methods are required (Hoeting, 1999). In dynamical systems simulation (i.e. Raftery et al, 2005; Duan et al, 2006), this problem has typically been solved iteratively as an expectation-maximization problem that simultaneously maximizes the likelihood of both $p(\Delta | M_k, Y_{obs})$ and w_k , though other approaches have been employed in other domains (i.e. Ker and Liu, 2020).

255 Generalized Likelihood Uncertainty Estimation (GLUE) is an approach to uncertainty estimation with wide use in hydrology (Beven and Binley, 2014). GLUE recognizes that discrepancies between observed and simulated data often exhibit non-random patterns, reflecting the presence of heteroscedasticity and autocorrelation resulting from errors in simulator

structure, inputs, and data (Beven, 2012). To account for these uncertainties, GLUE assigns a "measure of belief" to each simulation result reflecting confidence in its validity. This measure of belief, or likelihood function, may not be formal in the statistical sense but serves to express the practitioner's subjective judgement (Beven, 2012). The selection of an appropriate likelihood is crucial, often relying on performance metrics such as Nash Efficiency (NSE), but its choice depends on the study objective (Smith et al., 2008). Likelihoods are used to develop acceptability limits, weight a set of simulation results, and approximate the uncertainty associated with the inference of parameters. By allowing consideration of multiple simulator structures and developing a clear metric by which to evaluate them, GLUE provides a holistic and flexible framework for parameter estimation in the presence of error related to simulator structure and other epistemic uncertainties (Beven, 2012).

The current analysis adopts a strategy that combines SBI with informal likelihood weighting to address error related to the simulator structure. This approach involves generating weighted averages of estimated parameter distributions from a set of simulators with different underlying structures using a form of BMA (Eqn. 3). Specifically, we take the weighted average of the conditional estimates of $p(\theta|Y)$ (Eqn. 2) obtained through SBI for a set of surrogate rainfall-runoff simulators. As in GLUE, weights are calculated from a selected performance metric, reflecting the suitability of simulated given observed data; simulation results below a pre-defined limit of acceptability are not considered. The claim is that this method of combination mitigates over-confident inference due to simulator structural inadequacy without diluting the valuable information in the parameter estimates made by SBI. The broader implication is an approach to extend the usage of SBI to situations where some structural error related to the simulator is inevitable, as is often the case for real systems. We believe that being able to extend SBI in this way could, broadly speaking, be part of a strategy to build a more comprehensive understanding of the inherent uncertainties associated with hydrological modeling approaches. Experiment 4 evaluates whether BMA produces more accurate parameter estimates and realistic parameter spreads compared to standalone SBI. Refer to Section 3.8 for implementation details.

3 Materials and Methods

This section describes our implementation of surrogate-derived SBI, and four experiments undertaken to test it. We first introduce those experiments, and the goals associated with them (Sect. 3.1). Then, we describe the domain of interest, the Taylor River catchment (Sect. 3.2). The rest of the methods subsections describe the components, implementation, and validation of SBI, as outlined in Table 1.

Table 1. Outline of the components described in the methods section.

Section	Name	Description
3.1	Experiments	

3.2	Taylor River Catchment	Domain of study
3.3	ParFlow	Process-Based simulator
3.4	Long-Short Term Memory (LSTM) Network	Surrogate simulator
3.5	Simulation-Based Inference (SBI)	Method for parameter inference
3.6	Conditional Density Estimator, $q_\phi(\theta Y)$	Learns distribution of parameters
3.7	Posterior Predictive Check	From inferred parameters, make prediction
3.8	Calculation of Weights	Method for considering multiple simulator structures
3.9	Evaluation Metrics	Assess performance of SBI

285

Figure 1 shows how the components of surrogate-derived SBI interrelate. In Fig. 1A, a small set of process-based simulations are generated by ParFlow. A LSTM neural network learns from these simulations to mimic the behavior of ParFlow, interpolating the relationship between climate forcings, catchment parameters M and K and output streamflow time series. The LSTM can be used as a ParFlow surrogate to quickly explore the streamflow response to different parameter configurations and forcing scenarios. Throughout the rest of the paper we will refer to ParFlow as the PB simulator and the LSTM as the surrogate simulator or the LSTM.

We leverage the efficiency of the surrogate to conduct SBI on parameters, as depicted by Fig. 1B. Our goal with SBI is to estimate probable values for the catchment parameters M and K given the occurrence of a particular streamflow observation. To that end, we randomly sample many (n=5000) parameter configurations from a prior distribution $p(\theta)$ and from the LSTM simulate an equivalent number of streamflow time series Y . This set of simulated parameter-data pairs is used to train a neural density estimator $q_\phi(\theta|Y)$, which is a deep-learned model of the full conditional density of parameters given data $p(\theta|Y)$. Once trained, the neural density estimator is evaluated with a given observation to produce a distribution of parameters, the posterior distribution $p(\theta | Y = Y_{obs})$, which represents our ‘best guess’ of what the parameters should be. The prior distribution and other details of the density estimation approach are described in Table C1 and Section 3.5.

Finally, a predictive check (Fig. 1C) ensures that the parameter estimates generate a calibrated surrogate simulator. The simplest version of this check is to put the estimates of parameters from the previous step back into the LSTM, which generates a new ensemble of streamflow simulations. The simulations should resemble the observation closely if the simulator captures the behavior of the dynamical system well, and parameter inference was done correctly. Optionally, the parameter estimates may be weighted using a performance evaluation of the predictive check.

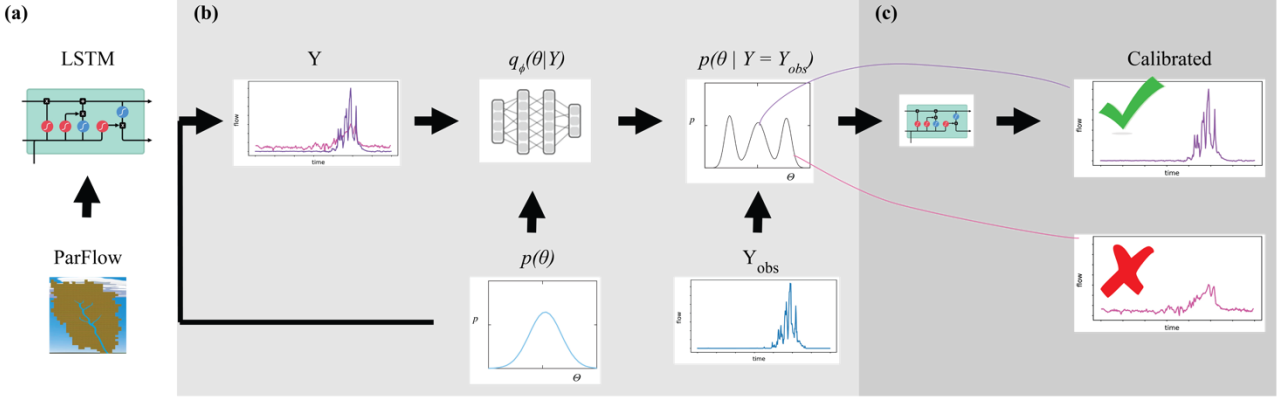


Figure 1. An illustration of surrogate-derived simulation-based inference (SBI). In subplot (a), a Long Short-Term Memory (LSTM) neural network learns catchment behavior from ParFlow, a process-based simulator. The implementation of SBI is shown in subplot (b), where the objective is to estimate catchment parameters θ given an observation Y_{obs} . This parameter estimate is formally known as the posterior parameter distribution $p(\theta | Y = Y_{obs})$. We randomly sample many parameter configurations from a prior distribution $p(\theta)$ and from the LSTM simulate an equivalent number of streamflow time series Y . This set of simulated parameter-data pairs is used to train a neural density estimator $q_\phi(\theta|Y)$. Subplot (c) shows the posterior predictive check, which involves using the parameter estimate to (ideally) generate a calibrated set of simulations.

310

315 3.1 Experiments

We explore the performance of SBI in four experiments. The subject of interest is the ability of SBI to accurately and precisely estimate parameters given observations under varying conditions of uncertainty. The uncertainty comes from error related to the structure of the surrogate simulator. Synthetic observations with known parameters are used to conduct the experiments because they are easier to benchmark; for completeness, the analysis is extended to actual catchment data in 320 Appendix E. To test SBI, we first draw the synthetic observations from the surrogate simulator, and then the harder-to-match PB simulator. Strategies to address uncertainty about the simulator structure and the effect on parameter estimates are presented in the final experiments. The experiments are further described in Table 2 and below, and the results are explored in Sect. 4:

325

1. ‘Best Case’: Find $p(\theta | Y = Y_{Obs_LSTM})$. We use as observation the streamflow generated by a surrogate simulator (e.g., with a given combination of parameters) and use SBI to infer the parameters. Because we are treating the simulator as observations in this case (i.e. we assume the simulator can generate data identical to the observation), no uncertainty exists about the structural adequacy of the simulator. This experiment serves as a baseline check for our SBI workflow.
2. ‘Tough Case’: Find $p(\theta | Y = Y_{Obs_ParFlow})$. We use a ParFlow simulation as observation and use SBI to infer the values of the parameters. As there is a slight mismatch between observed (in this case ParFlow simulation) and simulated data (i.e. the surrogate simulator), there is some uncertainty about the structural adequacy of the surrogate simulator.

This experiment tests whether the proposed framework, where SBI is carried out with the surrogate simulator, can be successful given misspecification of the surrogate.

335 3. ‘Boosted Case’: Find more accurate $p(\theta | Y = Y_{Obs_ParFlow})$. Building from the ‘Tough Case’, we again use a ParFlow simulation as observation but instead use an ensemble (‘boosted’) surrogate simulator to infer the known parameters. Unlike in the ‘Tough Case’, multiple forms of the surrogate simulator are considered to represent uncertainty about the appropriate structure. In this case we’re testing whether the proposed framework can be made more robust to surrogate misspecification if multiple surrogate structures are combined in an unweighted way.

340 4. ‘Weighted Case’: Find Bayesian Model Averaged $p(\theta | Y = Y_{Obs_ParFlow}, w)$. Building from the ‘Boosted Case’, we add a performance measure (e.g. informal likelihood) to emphasize (‘weight’) credible and reject implausible forms of the surrogate simulator that have been identified by SBI. Unlike in the ‘Boosted Case’, uncertainty about the adequacy of surrogate simulator structures and configurations is explicitly evaluated using the likelihood weighting. This experiment tests whether the proposed framework is more robust to surrogate misspecification if competing surrogate structures are weighted based on the fit between simulated and observed data.

345

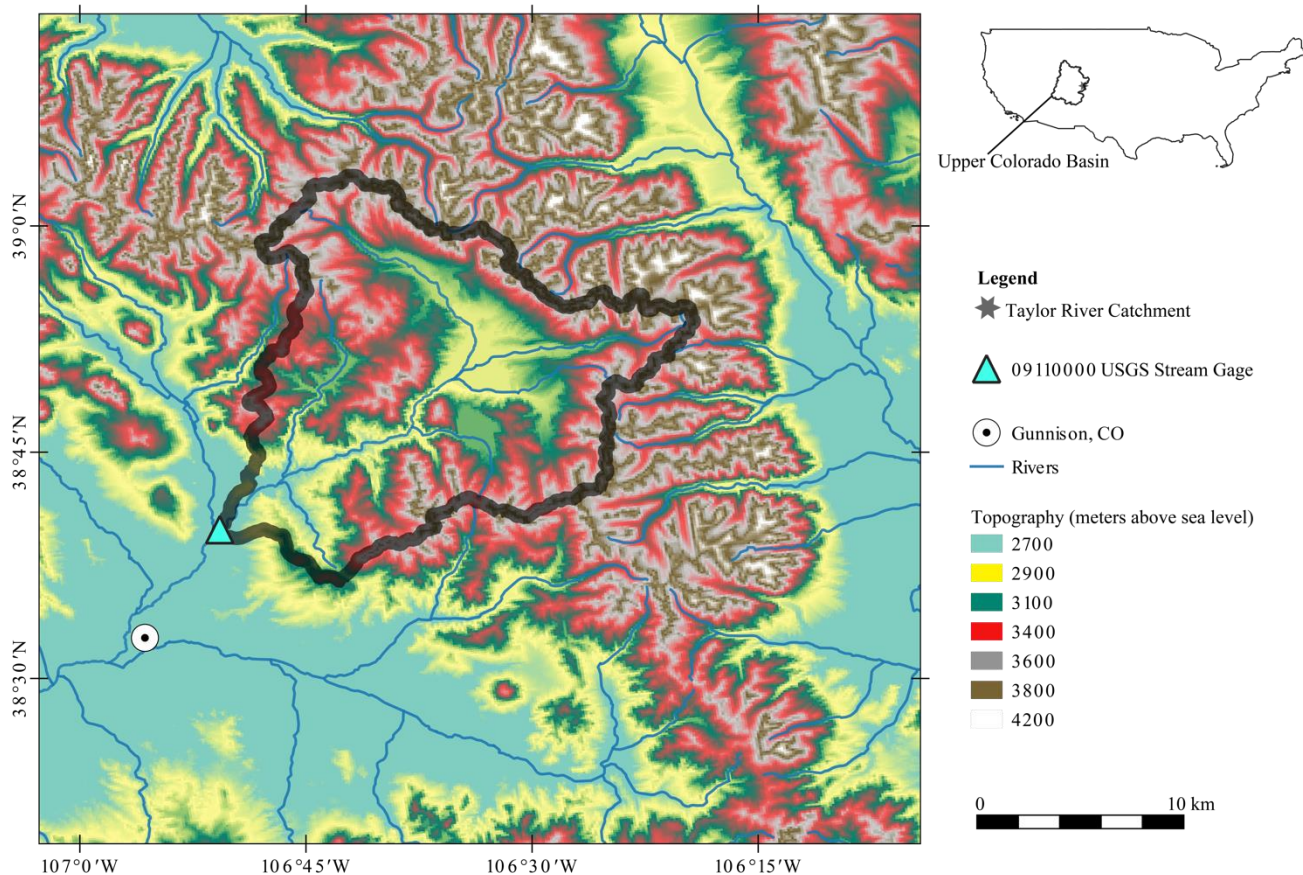
Table 2. The four experiments explore how the observation and simulator type affect the quality of parameter inference.

Experiment #	Name	Goal
1	<i>Best Case</i>	Infer parameters given no mismatch between observed and simulated data
2	<i>Tough Case</i>	Infer parameters given some mismatch between observed and simulated data
3	<i>Boosted Case</i>	Infer parameters given some mismatch between observed and simulated data if multiple surrogate structures are combined in an unweighted way.
4	<i>Weighted Case</i>	Infer parameters given some mismatch between observed and simulated data from multiple surrogate structures weighted by their goodness of fit.

3.2 Taylor River – The Domain

The physical area of study is the Taylor River headwater catchment located in the Upper Colorado River Catchment (Figure 350 2). The Taylor is an important mountain headwater system for flood control and water supply in the Upper Colorado River Catchment (Leonarduzzi et al., 2022). This catchment is at an elevation of between 2451 and 3958 meters above mean sea level and has a surface area of around 1144 km². This catchment is snowmelt-dominated in summer. The geographical extent of the catchment is defined by the USGS streamflow gage in Almont, Colorado (ID: 09110000) at the catchment outlet. Over the full period of record (1910 - 2022), the lowest average monthly discharges are recorded in January and February, with 355 values of approximately 100 [cfs] (3 [cms]), after which there is a steady increase of discharge and generally wetness in the

catchment up until June, when an average discharge of approximately 900 [cfs] (25 [cms]) is recorded. Synthetic data corresponding to the Almont gage (USGS 09110000) location are used for Experiments 1-4, as described in Sect. 3.1. Observed streamflow data from water year 1995 are revisited in the discussion and Appendix E.



360

Figure 2. Map showing the study domain Taylor River catchment near Almont, Colorado.

3.3 The Process-Based Simulations (ParFlow)

We use the integrated hydrologic simulator ParFlow-CLM to simulate groundwater and surface water flow in our 365 domain. ParFlow-CLM is designed to capture dynamically evolving interactions between groundwater, surface water and land surface fluxes (Jones and Woodward, 2001; Maxwell and Kollet, 2006; Maxwell et al., 2015a). In the subsurface, variably saturated flow is solved using the mixed form of Richards Equation. Overland flow is solved by the kinematic wave approximation and Manning's equation. ParFlow is coupled to the Common Land Model (CLM). CLM is a land surface model

which handles the surface water-energy balance (Maxwell and Miller, 2005; Kollet and Maxwell, 2008). It is thus well-suited
370 to examine evolving catchment dynamics at the large scales (e.g., Maxwell et al., 2015b), as in the Taylor River Catchment in
Colorado, USA.

The Taylor catchment is represented by ParFlow at 1 kilometer resolution, with five vertical layers of total depth 102
375 meters (Leonarduzzi et al., 2022). As with Leonarduzzi et al., 2022, all the required input files - including soil properties,
landcover, and meteorological forcings - are subset from Upper Colorado River Catchment ParFlow-CLM simulations of Tran
et al. 2022. The subsurface contains 23 separate soil and geological units.

We explore the sensitivity of streamflow to an ensemble of different configurations of Manning's roughness
coefficient (M), and hydraulic conductivity (K). For the baseline configuration of the simulator, K ranges between 6.2×10^{-3}
380 and 2.7×10^{-1} [m/h] across the 23 spatial units; M is constant across the domain surface at 2.4×10^{-6} [h/m^(1/3)]. An ensemble
of 183 simulations is generated by systematically varying M and K . For M since the values are spatially constant it is easy to
adjust this single value. K is spatially variable; therefore, we apply a single scaling factor to all three dimensions (Table A1).
To make the distinction clear, we call these 'single' scalar representations K_s and M_s , respectively. The values K_s and M_s used
in this study are shown in Table A2. A sensitivity analysis of streamflow to parameter configurations is shown in Fig. A1.

All simulations are run for a one-year period (8760 hours) using forcings from water year 1995 taken from Tran et
al., 2020. Surface pressure outputs are converted to runoff using the overland flow utility built into ParFlow. This study focuses
385 on runoff at the cell closest to USGS gage 09110000. We convert to cubic feet per second (cfs) for direct comparison to gaged
data and rescale from 0 to 1. Streamflow simulations from ParFlow are relatively more sensitive to changes in K than M , as
shown in Fig. A1. The relatively small size of the ensemble is due in part to the computational demand of ParFlow. The time
for each ParFlow simulation was 28 minutes. Since there are 183 simulations in the ensemble, the total simulation time was
about 85 hours. All simulations were undertaken in the Princeton Hydrologic Data Center (PHDC) on NVIDIA A100 GPUs.
390 The purpose of generating this ParFlow ensemble is not to create the most diverse set of system realizations but provide a
foundation from which to train the surrogate simulator and test performance of the simulation-based inference approach.

3.4 The Surrogate Simulator (LSTM)

We employ a Long Short-Term Memory (LSTM) network to learn from our process-based simulator ParFlow.
LSTMs are neural networks that are designed to learn temporal relationships (Rumelhart et al., 1986; Hochreiter and
395 Schmidhuber, 1997). LSTMs are widely used for predictive tasks in hydrology, for example to relate meteorological forcing
sequences (Kratzert et al. 2018) to catchment streamflow. In our study, an LSTM network learns the response of streamflow
at gaged location 09110000 to forcings and parameters in the Taylor River catchment, as defined by the ensemble of ParFlow
simulations described in Sect. 3.3.

Throughout our experiments, we used an LSTM with 10 input features containing forcings X and parameters θ , and
400 one output class containing streamflow Y . As in Kratzert et al. 2018, we employ a 'look-back' approach. For each sample, the

LSTM ingests a sequence length of ' l '=14 days of previous forcings weighted by scalar representations of ParFlow parameters (K_s , M_s) and returns streamflow the next day. More explicitly:

$$Y_{t+1} = LSTM(X_{t-(l-1)}, K_s, M_s) \quad (4)$$

where Y_{t+1} is the streamflow the next day, l is the 'look back' which controls the length of the input sequence used for prediction, $X_{t-(l-1)}$ are vectors containing sequences of forcing data from today (i.e., day t) back to day t minus l for each of the 8 forcing variables. K_s and M_s are scalar representations of the ParFlow parameters hydraulic conductivity (K) and Manning's roughness (M). Since these values do not vary over time each is ingested as a vector repeated ' l ' times by the LSTM.

The relevant hyperparameters used to fit the LSTM surrogate are further defined in Table A1 and B1. The computational cost of the LSTM is much less than the cost of ParFlow. The time for training the LSTM is around 15 minutes in the PHDC. Once trained, simulation from the LSTM is low cost (less than 6×10^{-5} seconds). Fig. B1A shows the distribution of train-validation and test sets across parameter space and the performance of the LSTM relative to ParFlow on a streamflow time series generated by a randomly selected test parameter set, θ_A is used throughout the results section for benchmarking. Hyperparameters were determined by trial and error. The LSTM captures the general streamflow behavior quite well, but not quite perfectly (Figure B1B). The Kling Gupta Efficiency (KGE) exceeds 0.7 for test data reserved from ParFlow. We emphasize that the goal here is to produce a surrogate simulator adequate for the simulation-based inference of parameters K_s and M_s .

3.5 Implementation of Simulation-Based Inference

The goal of SBI is to infer appropriate values flexibly and efficiently for simulator parameters, given a particular observation. SBI is illustrated in Fig. 1B. Take θ to be a vector of parameters that control a simulator, and let Y be a vector of simulated data. The simulator implicitly defines a conditional probability $p(Y|\theta)$, which may be analytically intractable. $p(\theta)$ encodes our prior beliefs about parameters. We are interested in inferring the parameters θ given an observation Y_{Obs} , i.e., we would like to know the posterior probability density $p(\theta|Y=Y_{Obs})$, after Papamakarios and Murray (2016):

$$p(\theta|Y = Y_{Obs}) \propto p(Y = Y_{Obs} | \theta) p(\theta) \quad (5)$$

where θ contains K_s and M_s , and Y_{Obs} is an 'observed' streamflow time series. Y is a set of simulated outputs that are formally equivalent but not identical to the observation Y_{Obs} . Here, parameter-data pairs are simulated by a surrogate (Sect. 3.4) of ParFlow. Simulations are drawn from the same forcing scenario to limit the degrees of freedom of parameter inference.

A conditional density estimator $q_\phi(\theta|Y)$ learns the posterior density directly from simulations generated by the surrogate. q_ϕ is a learnable model - often a neural network - that fits to $p(\theta | Y)$ and can be evaluated to approximate $p(\theta | Y =$

Y_{Obs}). (See section 3.6 for details about q_ϕ). The procedure can be summarized as follows, after Papamakarios and Murray, (2016):

1. Propose a *prior* set of parameter vectors $\{\theta\}$, sampled from $p(\theta)$.
2. For each θ , run the simulator to obtain the corresponding data vector, Y .
3. Train the neural density estimator $q_\phi(\theta|Y)$ on the simulated set from $\{\theta, Y\}$.
4. Evaluate q_ϕ at observed data vector Y_{Obs} to generate a *posterior* set of parameter vectors $\{\theta\}$ proportional to $p(\theta | Y = Y_{Obs})$.

The SBI workflow and architectures used in this study are derived from a python toolbox for simulation-based inference

(Tejero-Cantero et al., 2020). We direct the reader to Papamakarios and Murray (2016) for a detailed description of the structure, training, and evaluation of a neural conditional density estimator for simulation-based inference. Others (Lueckmann et al. 2017; Greenberg, Nonnenmacher, and Macke 2019) have built on this idea to introduce MCMC-like approaches to sequential learning of the posterior at observations to make inference more efficient. We employ a sequential learning procedure in our workflow, as described in Appendix C.2. The hyperparameters and architectures used in SBI are shown in

Table C1.

3.6 Neural Conditional Density Estimators for SBI

The conditional density estimator $q_\phi(\theta|Y)$ is an essential ingredient of SBI. The neural conditional density estimator differs from conventional neural networks (such as the LSTM) in two important ways. First, it learns a conditional probability distribution, as opposed to a function. Second, it represents the ‘inverse’ model – the probability of parameters given data $p(\theta | Y)$ – as opposed to the dependency of data on parameters, which is encoded in ‘forward’ simulators like ParFlow and its surrogate, the LSTM. Once trained, the neural conditional density estimator is evaluated with an observation to infer a distribution of plausible parameters, the posterior distribution $p(\theta | Y = Y_{Obs})$ (Fig. 1B).

Conditional density estimators create a model for “a flexible family of conditional densities”, parameterized by a vector of parameters (ϕ) (Papamakarios and Murray, 2016). Density estimator parameters are not to be confused with the parameters of PB simulators or its surrogate, θ . The latter are the target of inference while the former parameterize the density-estimated posterior probability and must be learned or derived to conduct inference of simulation parameters. Deep neural networks provide new opportunities to learn ϕ for complex classes of densities, which gives rise to the term *neural* conditional density estimator.

Mixture Density Networks (MDNs) are an intuitive class of conditional density estimators capable of modeling any arbitrary conditional density (Bishop, 1994). They take the form of a mixture of k (not hydraulic conductivity, K) Gaussian components, as below.

$$q_\phi(\theta|Y) = \sum_k \alpha_k \mathcal{N}(\theta|m_k, S_k) \quad (6)$$

465 where the mixing coefficients (α), means (m), and covariance matrices (S) comprise the neural density parameterization, ϕ .
They can be computed by a feedforward neural network.

Training an MDN is a maximum likelihood optimization problem (Bishop, 1994). Given a training set of N simulation parameters and data pairs, $\{\theta, Y\}$, the objective is to maximize the average log probability (or minimize the negative log probability) with respect to the parameters, ϕ .

470

$$\operatorname{argmax}_{\phi} \frac{1}{N} \sum_n \log q_{\phi}(\theta_n | Y_n) \quad (7)$$

For a fuller description of the parameterization and training of neural density estimators, see the supplementary material in Papamakarios and Murray (2016) or the original write-up in Bishop (1994). This study uses a specialization of this
475 family of neural networks called a Masked Autoencoder for Density Estimation, further described in Appendix C.1.

3.7 Posterior Predictive Check

A crucial diagnostic step in the SBI workflow is to check the ability of the simulator to characterize process(es) of interest after inference has been conducted (Cranmer et al., 2020). To be more explicit, this step checks that parameters from the inferred posterior $p(\theta | Y = Y_{Obs})$ can simulate streamflow data (Y) consistent with the observation (Y_{Obs}) when plugged
480 back into the simulator. The simulated data should ‘look similar’ to the observation (Tejero-Cantero et al., 2020). Gabry et al. (2019) describe this type of evaluation as a ‘posterior predictive check’. This predictive check is represented by Fig. 1C.

Here, we conduct posterior predictive checks by drawing a small number of parameter sets from our inferred parameter posterior density. In our workflow, the inferred posterior parameter density is represented by an array containing thousands ($n=5000$) of plausible parameter sets. The frequency of their occurrence is ‘probability weighted’, in the sense that
485 there are very few occurrences of parameter sets in the ‘tails’ and many occurrences close to the mean, and improbable parameter sets do not exist at all. For our posterior predictive check, we randomly sample ($n=50$) parameter sets from this frequency-weighted parameter posterior array. We use these parameter samples to generate an ensemble of ‘predicted’ streamflow time series using the LSTM.

3.8 Calculation of Weights

490 Bayesian Model Averaging (BMA) is a method of combining different simulator structures to reduce the risk of overfitting on prediction or inference (Madigan and Raftery, 1994). The implementation explored here uses an informal likelihood measure to assign probabilities, or weights, to the SBI-derived parameter estimates of some number of simulators. Note that the simulators could be PB or surrogates. The structure of each simulator may be unique, in that the mathematical
495 description of the relationship between streamflow and parameters θ differs. Specifically, the sets of parameters estimated by SBI are resampled using weights based on the fit of observed and simulated streamflow to estimate a new probability density.

Given a set of K models (M_1, M_2, \dots, M_K) defined implicitly by the simulators considered, this *weighted* estimated density $p(\theta|Y_{Obs}, w_k)$ is:

$$p(\theta|Y_{Obs}, w_k) = \sum_{k=1}^K p(\theta|M_k, Y_{Obs}) w_k \quad (8)$$

500 where $p(\theta|M_k, Y_{Obs})$ is equivalent to the posterior parameter density, $p(\theta|Y = Y_{Obs})$ from SBI (eq. 5); and w_k is the model probability or weight, which is based on the goodness of fit of simulated data from the posterior predictive check. All probabilities are implicitly conditional on the set of all models considered.

505 In the current application, weights are calculated using the informal likelihood L_{ik} for simulations drawn from the posterior predictive check. Simulations are defined as values for parameters θ and resulting simulated data Y . The informal likelihood is a measure of acceptability for each simulation result based on its error relative to observed data. Simulations with likelihood measures below a pre-defined limit of acceptability are rejected; the set of remaining simulations is assumed to be equally probable prior to weighting. Weights for each simulator in the set K of structures, each composed of a set of I simulations, is equal to:

$$w_k = \frac{L_{ik}}{\sum_{k=1}^K \sum_{i=1}^I L_{ik}} \quad (9)$$

510 The informed reader will recognize disagreement and inconsistent usage in the literature about the likelihood function (Beven, 2012; Nearing et al, 2015). We acknowledge legitimacy in all camps, but here adopt a subjective, or informal, likelihood as sometimes used in Generalized Likelihood Uncertainty Estimation (GLUE). We choose to use the Kling Gupta Efficiency (KGE; Gupta et al., 2009) as the likelihood metric for its utility and history rainfall-runoff simulation. Furthermore, we note that the method is not dependent on a specific metric and others could apply this approach using a different metric if they choose. The KGE metric is computed using the following equation:

$$520 \quad KGE = 1 - \sqrt{(1 - \alpha)^2 + (1 - \beta)^2 + (1 - \rho)^2} \quad (10)$$

Where α is the ratio of the standard deviation of simulated and observed streamflow data, respectively; β is the ratio of their means; and ρ is the correlation coefficient in time.

525 The *weighted* probability density $p(\theta|Y_{Obs}, w_k)$ is estimated using a distribution sampling algorithm, where the distribution represents the weights of each simulation i under each simulator k . Simulation indices are sampled by mapping a random target probability between 0 and 1 to the cumulative distribution of simulation weights. This approach can be used to sample sets of parameters from the SBI-inferred posterior parameter density weighted to high-likelihood simulations identified by the posterior predictive check.

3.9 Evaluation Metrics

530 The performance of simulation-based inference is evaluated in terms of accuracy and precision. First, we evaluate performance with respect to the parameter posterior (the inferred parameters); and second with respect to the posterior predictive check (the ability to generate realistic data using the inferred parameters).

3.9.1 Evaluating the Posterior Parameter Density

535 Accuracy of parameter inference is evaluated using the Mahalanobis distance, $D_M(\theta_{True})$. Mahalanobis distance measures the distance between a point and a distribution of values after Maesschalck et al. (2000), such that:

$$D_M(\theta_{True}) = \sqrt{(\theta_{True} - \theta_\mu)^T \Sigma^{-1} (\theta_{True} - \theta_\mu)} \quad (11)$$

540 where θ_{True} is the set of observed or ‘true’ parameters; θ_μ is the mean of the posterior distribution $p(\theta | Y = Y_{Obs})$; and Σ is the covariance matrix of $p(\theta | Y = Y_{Obs})$. In essence, Mahalanobis distance measures how far off our parameter estimate is from the ‘truth’. For this study values less than two are defined as acceptable (within ~two standard deviations); this threshold was identified via trial and error.

545 Precision of parameter inference is evaluated in terms of the determinant of the covariance matrix of the inferred parameter posterior, $|\Sigma|$. The determinant can be interpreted geometrically as the ‘volume’ contained by the covariance matrix, and by extension the inferred parameter posterior distribution. Larger determinant values are less precise; smaller values more precise (4.3 Determinants and Volumes). In this study we define values less than 10^{-6} as acceptable, identified via trial and error.

3.9.2 Evaluating the Posterior Predictive Check

550 We evaluate the ability of the simulated ensemble of streamflow to adequately characterize the observed streamflow using the root mean squared error (RMSE) between each (n=50) simulated streamflow time series (Y) and the observed streamflow time series (Y_{Obs}). RMSE is calculated for each predication as the square root of the mean squared error, such that:

$$RMSE(Y) = \sqrt{\frac{\sum_{t=1}^T (Y_t - Y_{Obs,t})^2}{T}} \quad (12)$$

555 where $Y_{pred,t}$ is the simulator-predicted streamflow at time t , taken from Y_{pred} ; $Y_{Obs,t}$ is the observed or true streamflow at time t , taken from Y_{Obs} ; T is the number of times (days) in the streamflow time series.

Accuracy of the simulator characterization of streamflow is the mean of the RMSE calculated for all n=50 Y relative to Y_{Obs} ($RMSE_{Ave}$). Precision of the simulator characterization of streamflow is assessed as the standard deviation of the RMSE calculated for all n=50 Y_{pred} relative to Y_{Obs} ($RMSE_{std}$). For both the mean and variance RMSE values less than 0.01 [scaled

streamflow units], identified via trial and error, are acceptable. RMSE was selected to evaluate the posterior prediction out of

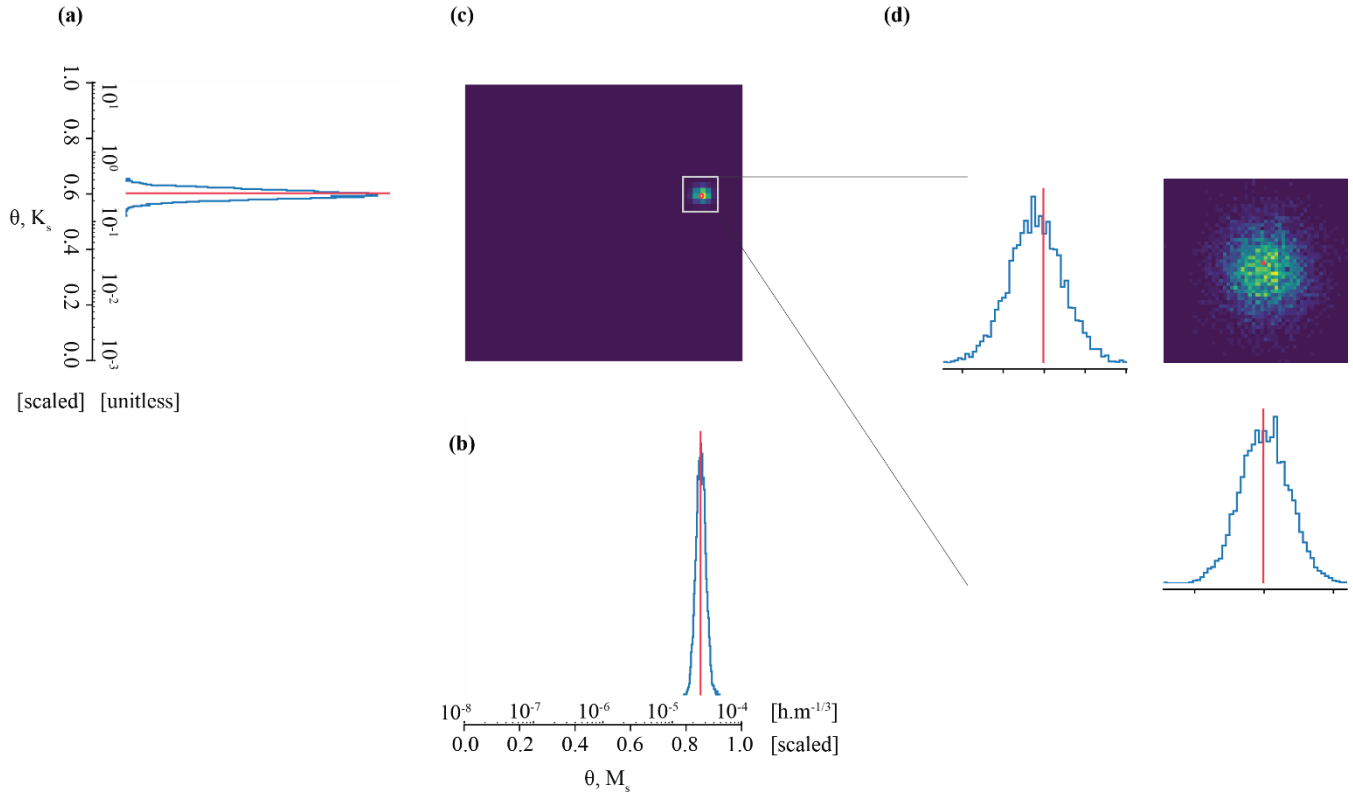
560 convenience. Other metrics, such as KGE, could also be used.

4 Results

Here we present the outcomes of the three experiments described in Sect. 3.1. The first two experiments showcase inference problems that increase in difficulty from the easy *best case* (Sect. 4.1) to the hard *tough case* (Section 4.2). The final experiments offer workarounds by way of the *boosted case* (Sect. 4.3) and *weighted case* (Sect 4.4). The performance of the 565 methods explored in the three experiments is first discussed in terms of one shared benchmark scenario. Then, we show the results of the three experiments on a larger shared set (n=18) of benchmark scenarios (Sect. 4.5).

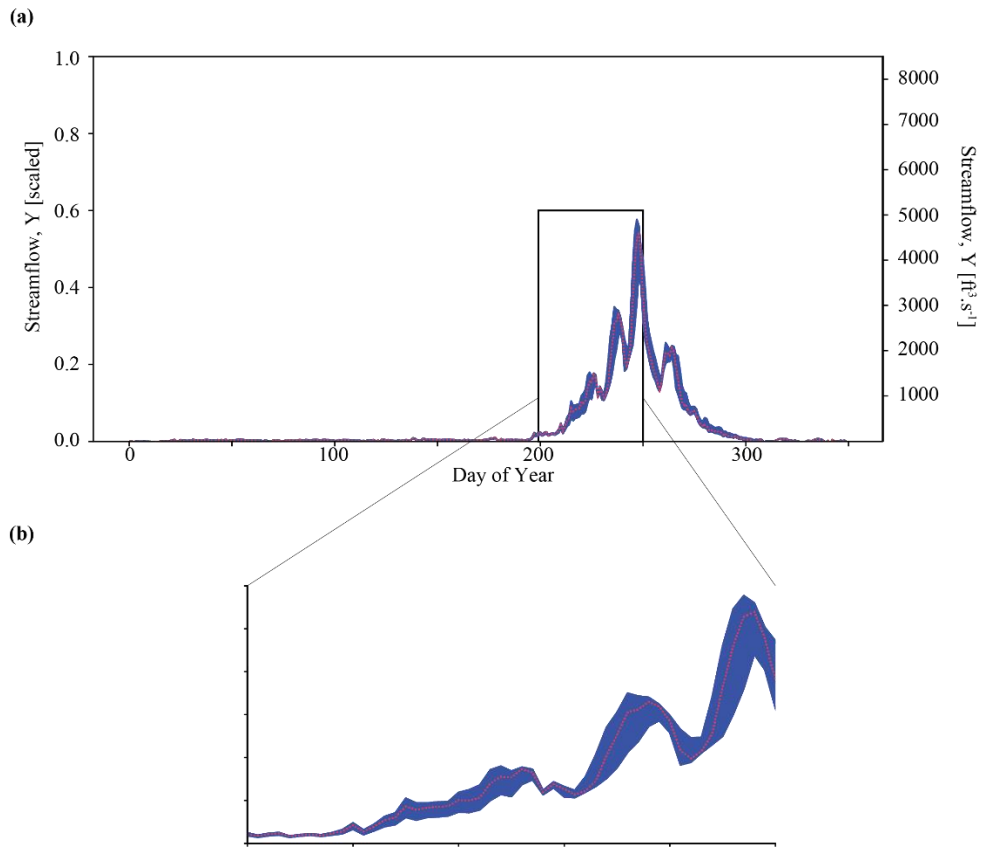
4.1 Experiment 1 – Best Case

For the *Best Case* scenario, we attempt to infer the parameters of synthetic observation(s) taken from the trained surrogate simulator, such that $p(\theta | Y = Y_{Obs_LSTM})$. We first infer the parameters of just one randomly selected streamflow 570 observation, denoted with an ‘A’ ($Y_{Obs_LSTM_A}$). The set of ‘benchmark’ parameters (θ_A) used to generate the underlying simulation are approximately 0.60 for K_s , and 0.85 for M_s . θ_A is also our benchmark in parameter space for Experiments 2 and 3.



575 **Figure 3.** The parameter posterior estimate for observation $Y_{\text{Obs_LSTM_A}}$ closely matches the true parameter values in the ‘best’ case. Subplots (a), (b) and (c) comprise a pair plot of posterior densities across the full possible parameter space; subplot (d) is zoomed in for detail. The posterior density of M_s (a) and K_s (b) are shown individually, and together (c). Axes are expressed in both the scale/transformed and unscaled units of the parameters. The ‘true’ parameters are denoted by the red line and circle, respectively.

580 We accurately and precisely estimate parameters for our benchmark case (Figure 3). The pair plot approximates the posterior parameter density evaluated by the neural density estimator at the observation. In individual parameter space, narrower peaks (in blue) correspond with more confident and precise parameter estimates. In shared parameter space (c), zones of deep purple are effectively zones of no probability; zones of blue-green-yellow are zones of high probability. The benchmark parameters (i.e., the parameters used to generate the simulation) are denoted by the red line and circle, respectively. Accuracy
585 is evaluated by the Mahalanobis Distance, which is 3×10^{-1} ; thus, the ‘true’ parameter set can be thought of as less than one ‘standard deviation’ from the central tendency of the inferred distribution. Precision is estimated by taking the determinant of the covariance matrix. The determinant of the covariance matrix is 9×10^{-8} . This is well below our threshold of 1×10^{-6} for sufficiently precise parameter inference.



590 **Figure 4.** Results of the posterior predictive check on synthetic observation $Y_{\text{Obs_LSTM_A}}$ in Experiment 1 ('base' case). Subplots (a) shows streamflow simulations resulting from inference of $p(\theta|Y = Y_{\text{Obs_LSTM_A}})$. The ensemble of predictions is bounded by blue, and observation in red. Blue lines represent time series of upper- and lower- streamflow values in this ensemble, and the red line represents the observation $Y_{\text{Obs_LSTM_A}}$. In subplot (b), we zoom into the area of greatest uncertainty between days 200 and 300, which correspond to the spring snow melt-off.

595

Taking this one step further we can use the inferred parameter distributions to generate an ensemble of streamflow simulations using the LSTM and compare this to the observed streamflow (referred to as our posterior predictive check). As show in Figure 4a, the inferred parameters generate simulation results that characterize the observed streamflow observation 600 reasonably well. Greater uncertainty exists around higher streamflow values over the course of the water year, as shown by the increasing width of the uncertainty envelope after day 200 (Figure 4B). Note that this is the time of year during which the increasing width of the uncertainty envelope after day 200 (Figure 4B). Note that this is the time of year during which snow melt-off occurs in the Taylor River Catchment. Mean and standard deviation of streamflow error are approximately 6×10^{-3} and 4×10^{-3} [scaled streamflow units], respectively.

Inference for many observations

605

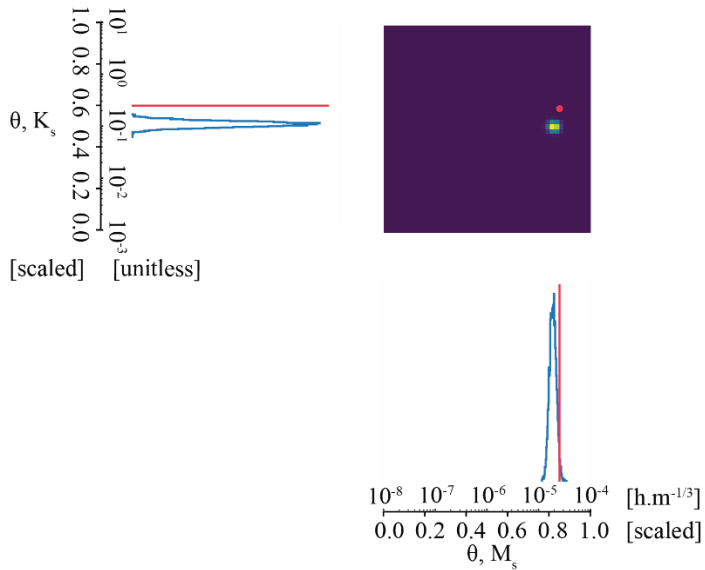
In addition to conducting this analysis for one observation as described, an advantage of SBI is the low computational expense of evaluating new observations. Simulations from the process-based simulations (i.e., ParFlow) are slow and scale

linearly with the number of simulations. It takes $\sim 10^5$ times longer to generate a ParFlow simulation (1680 seconds) than to evaluate one observation Y_{Obs} using a trained neural density estimator (0.045 seconds) on a high-performance computer system allocation of one CPU node with four gigabytes of working memory. Put another way, after an upfront sunk cost to learn the distributions, we can evaluate new observations, Y_{Obs} , practically for free. Many other techniques to parameter determination are not ‘amortized’ in this way (Cranmer et al., 2020). For example, Approximate Bayesian Computation (ABC) requires restarting most steps in the inference process when new data comes available (Vrugt and Sadegh, 2013). This property of SBI can be handy in domains where the system structure (parameters) stays the same, but new observations come available all the time - as can be the case in catchment hydrology. In Appendix D, we extend Experiment 1 to evaluate the posterior parameter density for many synthetic observations ($Y_{Obs_LSTM_i}$).

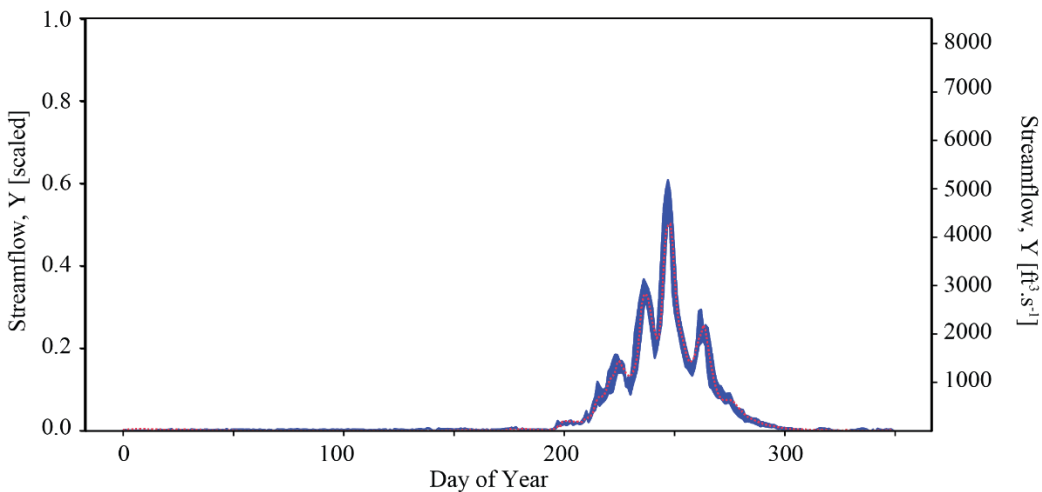
4.2 Experiment 2 – Tough Case

Experiment 2 is our *tough case*. We attempt to infer the parameters of synthetic observations from ParFlow, such that $p(\theta | Y = Y_{Obs_ParFlow})$. We do this using the same realization of the neural density estimator from Experiment 1 (the *best case*). The ‘tough’ case is a realistic test of the robustness of parameter inference. Specifically, it tests our ability to evaluate data from a different source. Unlike in the *best case*, we must deal with uncertainties related to the goodness of fit between the simulator (the LSTM surrogate) and ‘observation’ (the underlying ParFlow simulator). We generate the posterior parameter and predictive densities to the benchmark case (θ_A) explored in Experiment 1. The only difference is that $Y_{Obs_ParFlow_A}$ is a simulation generated by ParFlow, and not the surrogate.

(a)



(b)



625

Figure 5. Results of parameter inference and posterior predictive check on synthetic observation $Y_{\text{Obs_ParFlow_A}}$ in Experiment 2 ('tough' case). Subplots (a) and (b) show overconfident parameter inference that still results in well-constrained posterior predictive check.

630

Figure 5 plots the results of experiment two. Here we see that the quality of inference is somewhat degraded for the *tough case* compared to the *best case*. Parameter inference here is overconfident; it is precise but biased as indicated by the tight probability distributions and the difference between the peak probability and the observation (indicated by the red line in Figure 7A). The true parameter value does not plot in the area corresponding to highest probability. The determinant is 6×10^{-8} , which is within the same order of magnitude as the *best case*. However, the Mahalanobis Distance is much higher, at 7×10^{-6} .

635

Thus, the 'true' parameter set can be thought of heuristically as approximately seven 'standard deviations' from the central

tendency of the inferred distribution. Visual inspection of Figure 7B shows that streamflow simulations yielded by inferred parameters still characterize the synthetic streamflow observation well. However, average error is roughly twice as high for the *tough case* compared to the *best case* (1×10^{-2} compared to 6×10^{-3}), which is approximately equal the acceptability criterion described in Sect. 3.7.

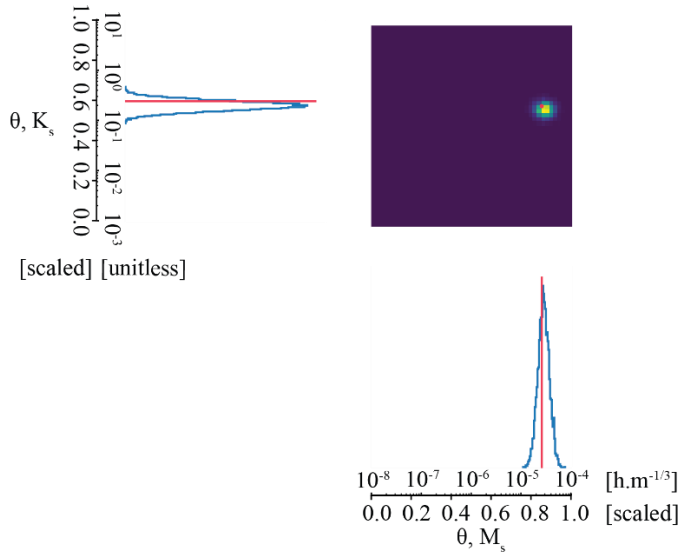
640 Overconfident posterior estimates are a result of the misfit between our LSTM surrogate compared to ParFlow (Figure B1B). One interpretation of overconfident parameter inference is that the relationship between data (streamflow) and parameters (M_s, K_s) in the LSTM surrogate does not *quite* represent their relationship as it exists in ParFlow. These differences are not unexpected, because ParFlow has parameters that vary across a three-dimensional domain but are lumped together in the LSTM (See also Appendix A). This bias in the surrogate simulator increases the possibility of overconfidence in the 645 conditional density learned by the neural density estimator. We consider this suboptimal performance in parameter inference a consequence of ‘surrogate misspecification’, as described further in Sect. 6.

4.3 Experiment 3 – Boosted Case

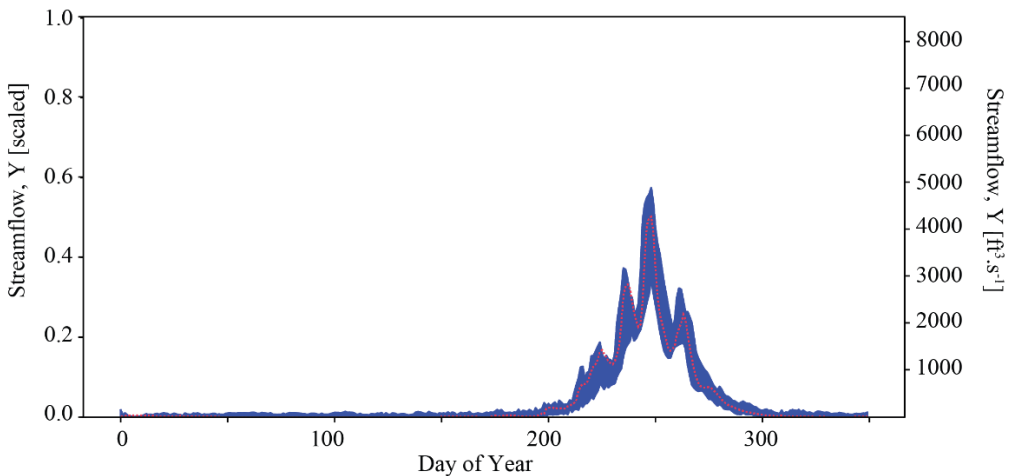
To prevent overfitting by the neural density estimator and circumvent overconfident parameter posteriors, we may use multiple ‘weak’ LSTM surrogates as opposed to one ‘strong’ surrogate. We utilize an ensemble of surrogate LSTM 650 simulators with distinct bias stemming from surrogate misspecification subject to the initialization and selection of training data. That ensemble is then used to generate the set of simulated pairs $\{\theta, Y\}$ to train a new neural density estimator. The underlying principle is that the overall behavior of an ensemble of surrogate simulators *in aggregate* may not be biased, even if each individual simulator has its own bias.

Experiment 3 is our *boosted* case. As in Experiment 2, we attempt to infer the parameters of synthetic observation(s) 655 reserved from ParFlow, $p(\theta | Y = Y_{Obs_ParFlow})$. As opposed to Experiments 1-2, we learn the conditional probability from an ensemble of 10 surrogate LSTM simulators instead of just one. We refer to the LSTM ensemble as a ‘boosted’ surrogate. Compared to the LSTM used in Experiment 1 and 2, these LSTMs are trained for fewer epochs (100, as compared to 300) and on a smaller random split of the data (0.7, as compared to 0.6). The reserved test data is the same across the LSTMs for 660 Experiments 1, 2, and 3. Note that we don’t use an adaptive learning algorithm such as AdaBoost (Freund and Schapire, 1997), and instead we equally weight each ‘weak’ LSTM simulator. The neural conditional density estimator is trained by taking a random draw from the ensemble of LSTMs and using the selected LSTM to generate a forward simulation of streamflow from a randomized parameter combination. Thousands of such draws are repeated until the conditional density has been sufficiently learned (see Appendix B for details), at which point it can be utilized for parameter inference.

(a)



(b)



665 **Figure 6. Results of parameter inference and posterior predictive check on synthetic observation $Y_{\text{Obs_ParFlow_A}}$ in Experiment 3** ('boosted' case). Subplots (a) and (b) show accurate parameter inference that is somewhat less precise, resulting in a wider but still well-constrained posterior predictive check.

670 Results of the *boosted case* in Experiment 3 show that we may be able to work around the issue of overconfident posteriors encountered in the *tough case* in Experiment 2. Fig. 6A shows precise and accurate parameter inference for our benchmark case in Experiment 3. The benchmark parameter values are in the area identified by the highest probability, as opposed to in Experiment 2. We note that the area of highest density is somewhat larger than in Experiment 2. The determinant is 5×10^{-7} , which is about an order of magnitude higher than the *tough case*, 6×10^{-8} . The Mahalanobis Distance is 1e0. For comparison, Mahalanobis Distance in the previous 'overconfident' experiment was 7e0. The inferred parameters generate

675 streamflow simulations that characterize the synthetic streamflow observation well, as shown by the posterior predictive check (Fig. 6B). We note that compared to Experiment 2 (Figure 5B) our simulations are somewhat more variable, as shown by the larger distance between the minimum and maximum simulated data. The average streamflow error is about twice as high for the *boosted case* as compared to the *tough case*, (2×10^{-2} compared to 1×10^{-2}). The standard deviation of the error is also greater (5×10^{-3} compared to 2×10^{-3}). The sacrifice in precision with respect to both parameter inference and the posterior prediction is a consequence of using an ensemble of surrogates to simulate each parameter set.

4.4 Experiment 4 – *Weighted Case*

In the preceding Experiment, we aimed to rectify overconfident parameter estimates arising from SBI due to surrogate misspecification. Adding an informal likelihood measure to the inferential paradigm may help to address the issue of overconfident parameter estimates by decreasing the importance of low credibility simulator structures. Experiment 4 685 demonstrates our *weighted* case. As in Experiments 2-3, we attempt to infer the parameters of synthetic observation(s) reserved from ParFlow, $p(\theta | Y = Y_{Obs_ParFlow})$. We extend the competing set of surrogate simulators from Experiment 3, each with distinct misspecification relative to ParFlow, to train a set of neural density estimators. These are evaluated with the synthetic observations to generate posterior parameter estimates and the associated posterior predictive check for each simulator considered. As opposed to Experiments 1-3, we use the Kling Gupta Efficiency (KGE) of the simulated data drawn from the 690 posterior predictive check to weight the importance of each set of inferred parameters. The added metric, the informal likelihood, emphasizes credible simulator structures and simulations (values for parameters θ and resulting simulated data Y), and safeguards against those that deviate significantly from observations. Simulations scoring less than persistence (defined by setting next week's predicted data equal to today's observed data) are considered not credible and assigned a weight of zero. The weights, w , are used to condition sampling from $p(\theta | Y = Y_{Obs_ParFlow})$. Weighted sampling yields a new set of inferred 695 parameters $p(\theta | Y = Y_{Obs_ParFlow}, w)$. We term this quantity the weighted posterior parameter density, an output of the methodology described in Section 3.8.

Table 3 characterizes the parameter estimates from the set of competing surrogate simulators and posterior density estimates for the benchmark scenario, $Y_{Obs_ParFlow}$ and θ_A . Each simulator is a separate row, with the resultant *weighted* outcome last. Some surrogate simulators are more credible than others, where credibility is represented by the average KGE of simulated 700 data taken from the posterior predictive check for each surrogate. The average KGE (second column) for most simulators clusters above 0.90, and for 7 and 9 is near a perfect match of 1. Simulators 3 and 6, with average KGE below 0.80, are generally less credible. The *weighted* KGE of 0.94 (Table 3, second column) indicates that the performance of the *weighted* outcome most resembles the most-credible simulators, but also incorporates information from less-credible ones.

705

Table 3. Calculation of the weighted posterior density from a set of competing surrogates for baseline synthetic observation $Y_{Obs_ParFlow_A}$.

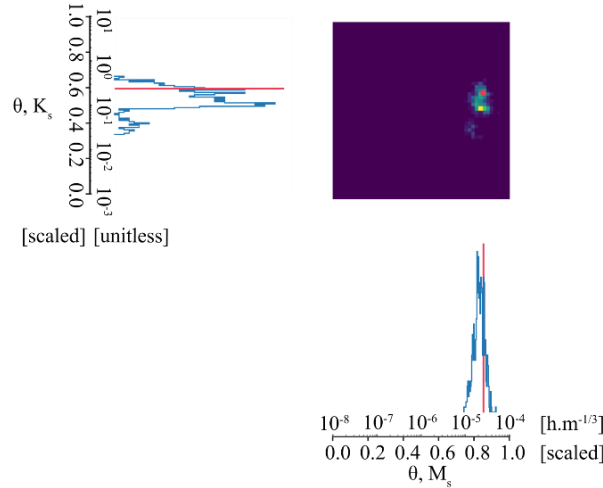
Simulator ¹	KGE ²	Cumulative Weight (%) ³	Rejections (%) ⁴	D _M ⁵	\Sigma ⁵
9	0.97	13.5%	< 0.200 %	3.8	2.9 x 10 ⁻⁷
7	0.97	13.4%	< 0.200 %	0.3	7.2 x 10 ⁻⁸
5	0.96	13.3%	< 0.200 %	2.3	1.4 x 10 ⁻⁷
4	0.96	13.2%	< 0.200 %	5.4	1.2 x 10 ⁻⁷
8	0.95	13.1%	< 0.200 %	4.6	1.2 x 10 ⁻⁷
2	0.90	12.4%	< 0.200 %	3.8	1.3 x 10 ⁻⁷
0	0.86	11.7%	2.20%	1.7	1.2 x 10 ⁻⁷
1	0.85	9.34%	23.0%	7.0	7.5 x 10 ⁻⁷
3	0.78	0.045%	99.6%	4.5	1.7 x 10 ⁻⁷
6	0.77	< .00100%	100.0%	6.6	1.8 x 10 ⁻⁷
Weighted ⁶	0.94	--	--	1.1	3.0 x 10 ⁻⁶

1. Competing surrogate simulators and the probability densities they implicitly define (n=10).
 2. Average Kling Gupta Efficiency (KGE) calculated from unweighted posterior predictions.
 3. Each posterior predictive simulation is weighted by the associated KGE; simulation weights are zero where poorer than persistence (KGE<0.81). The value in this column is the sum of the individual weights of 5000 predictive simulations taken for each surrogate.
 4. Count of rejected (zero weight) simulations divided by the total number of simulations for each surrogate.
 5. Mahalanobis Distance, D_M, and determinant, |\Sigma|, calculated by comparing are θ , $M_s = 0.85$ and $\theta_A K_s = 0.60$ to the unweighted parameter posterior $p(\theta | Y = Y_{Obs_ParFlow_A})$ for each surrogate
 6. The weighted posterior parameter density $p(\theta | Y = Y_{Obs_ParFlow}, w)$, derived by resampling the posterior densities using individual weights.

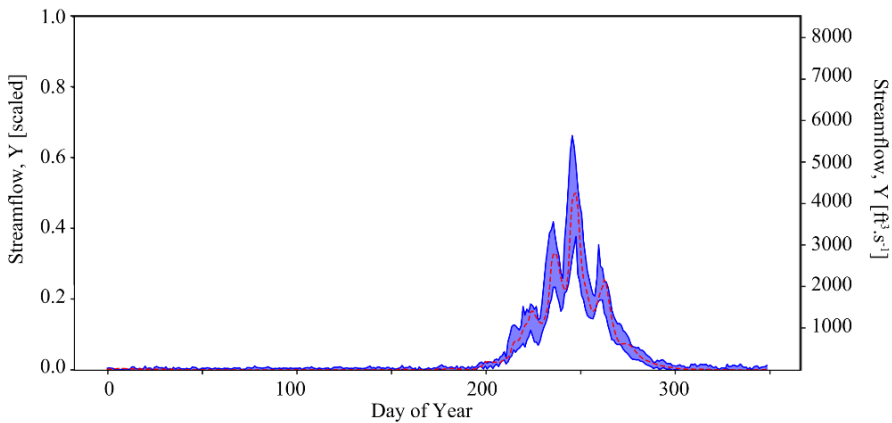
The simulator weights, which are calculated from individual simulation KGEs, are presented in the third column. The simulators that produce many credible simulations have a higher weight. Because predictive checks from simulators 8, 4, 5, 7, and 9 contain an equivalent number of credible simulations, they are nearly equally weighted. Surrogates 1, 3, and 6 have many rejected simulations, which are assigned a weight of zero. The percent of simulations drawn from the posterior predictive check for each simulator with KGE less than the limit of acceptability (0.81) is shown in the fourth column,

The relative accuracy of parameter estimates is presented in the fifth column as the Mahalanobis Distance, D_M, of the posterior parameter density for each surrogate. The parameter estimates derived from the *weighted* posterior density are more accurate than those drawn from all but simulator 7. This increase in accuracy reflects in part that higher-weighted members are associated with more-accurate parameter estimates compared to those that are lower-weighted. Note that the weighted parameter estimate is also less precise compared to that of the individual surrogates, as represented by the determinant |\Sigma| in column six.

(a)



(b)



730 **Figure 7. Results of parameter inference and posterior predictive check on synthetic observation in Experiment 4 ('weighted' case). Subplot (a) shows accurate parameter inference that is somewhat less precise and discontinuous, focused on simulator structures that are associated with a higher informal likelihood. The result is a narrow, well-constrained posterior predictive check in (b).**

735 Results of the *weighted case* in Experiment 4 demonstrate that it is a viable approach to the issue of overconfident posteriors encountered in the *tough case* in Experiment 2. Fig. 7A shows accurate parameter inference for our benchmark case in Experiment 4. As in Experiment 3, the benchmark parameter values are in the area identified by the highest probability. The Mahalanobis Distance, 1.1, is like that of Experiment 3. The geometry of the area of the highest density differs from Experiment 3, covering a larger area due to differences in the unweighted parameter estimates associated with each surrogate. As a result, the parameter estimate is less precise: the determinant $|\Sigma|$ is 3×10^{-6} , which is about an order of magnitude higher

740 than the *boosted case*, 5×10^{-7} . The inferred parameters generate streamflow simulations that characterize the synthetic

streamflow observation well, as shown by the posterior predictive check (Fig. 7B). We note that compared to Experiment 3 (Figure 6B) our simulations are about as variable. The average streamflow RMSE is similar for the *boosted case* as compared to the *weighted case* (2×10^{-2}). The standard deviation of the error is also very similar (5×10^{-3} compared to 6×10^{-3}).

4.5 Summary of Experiments 1-4

745 Previously, we compared the performance of simulation-based inference in Experiments 1 (*best case*), 2 (*tough case*), 3 (*boosted case*), and 4 (*weighted case*) on only one benchmark parameter set. In this section, we expand the comparison of SBI across the experiments to a larger number (n=18) of parameter sets and corresponding observations. In the case of Experiments 1 and 2, the same neural density estimator was utilized to conduct inference. For Experiment 3, an ensemble approach was used to create one new neural density estimator; for Experiment 4, likelihood-weighted parameter estimates 750 from an ensemble of neural density estimators was used. In the case of Experiments 2- 4, the mock data are the same benchmark streamflow simulations from ParFlow; for Experiment 1, the observations are taken from the surrogate. All four experiments utilize mock data corresponding to the same test parameter sets, to make an apples-to-apples comparison. For reference, those test parameter sets are plotted relative to parameter space in Fig. B1A. The results of the analysis of multiple (n=18) parameter sets are shown by the box plots in Fig. 8.

755 4.5.1 The precision and accuracy of parameter inference

In general, the parameter estimates from the four experiments are accurate and precise, as shown in Fig. 8A and 8B. The *best case* (Experiment 1) tends to be both precise and accurate. Compared to Experiment 1, the *tough case* (Experiment 2) tends to be just as precise but less accurate, while the *boosted case*. This is to be expected as we made the problem harder for Experiments 2-4 by not assuming a perfect surrogate. Experiment 3 tends to be less precise but more accurate than 760 Experiment 2. Compared to Experiment 3, the *weighted case* (Experiment 4) tends to be yet less precise and more accurate. A couple of second-order discussion points arise from Figs. 8A and 8B.

The resulting box plots of the determinant, a metric for the precision of inference, are shown in Fig. 8B. Here we see that the training of the conditional density estimator – and not the source of the observations – seems to define the precision of inference. The box plots show parameter inference is more precise (i.e., the determinant smaller) for Experiments 1 and 2, 765 compared to Experiments 3 and 4. Experiments 1 and 2 use synthetic observations from different sources (the LSTM surrogate and ParFlow, respectively), however they are both evaluated using the same neural conditional density estimator; note the similar behavior of the determinant in the first two experiments. On the other hand, the determinant behaves quite differently in Experiment 2 compared to Experiments 3 and 4; all three experiments use synthetic observations from ParFlow but use different configurations of the neural conditional density estimator. In the case of Experiment 3 (the *boosted case*), differences 770 within an ensemble of LSTM surrogates are lumped into the training of one neural density estimator; in the case of Experiment 4 (the *weighted case*), those differences are incorporated in the training of separate neural density estimators. Results show that Experiment 3 is associated with greater precision in parameter inference (i.e. smaller determinant) compared to Experient

4, as shown by the expanded volume of the parameter estimates in Figs. 7A compared to 6A. The lumping approach in the
775 *boosted case* may smooth differences between the surrogates, de-emphasizing parameter combinations in the tails of the separated posterior densities used in the *weighted case*. The likelihood-weighting and limits of acceptability also influence the distribution of the parameter estimate, but not in a manner that significantly decreases its precision. More fundamentally, the precision of parameter inference for those methods seems to reflect the simulator(s) (i.e., the variety in simulated responses, Y , to parameter configurations, θ), and not contain much, if any, information about the goodness-of-fit between observations, Y_{obs} and simulated data, Y .³

780 Box plots of the Mahalanobis⁴ distance, a metric of the accuracy of inference, are shown in Fig. 8A. The box plots show that parameter inference in Experiments 2 and 3 degrade in accuracy compared to Experiment 1, while parameter inference from Experiment 4 is nearly as accurate. The box plots also demonstrate that parameter inference is in general more accurate for the *boosted case* (Experiment 3) compared to the *tough case* (Experiment 2). However, the Mahalanobis distance is greater at some outlier points in the *boosted case* (Figure 7B). What this means is that while the *boosted case* yields more
785 accurate inference in some parts of parameter space (for example, the benchmark parameter set θ_A explored throughout the earlier results sections), this implementation is no silver bullet for averting overconfident parameter estimates. On the other hand, the *weighted case* introduced in Experiment 4 is consistently associated with much smaller Mahalanobis distances compared to either the *tough* or *boosted* cases. The apparent accuracy of the *weighted case* can be attributed to the likelihood-based weighting and limits of acceptability methodology, as well as the decrease in precision due to drawing from a set of
790 competing density estimates.

³ This behavior is also observed in Figure D1A, which shows that the determinant exhibits a fixed pattern across parameter space.

⁴ Note that Mahalanobis distance is a precision-weighted metric of distance, unlike Euclidean distance. These numbers should not be considered raw distance.

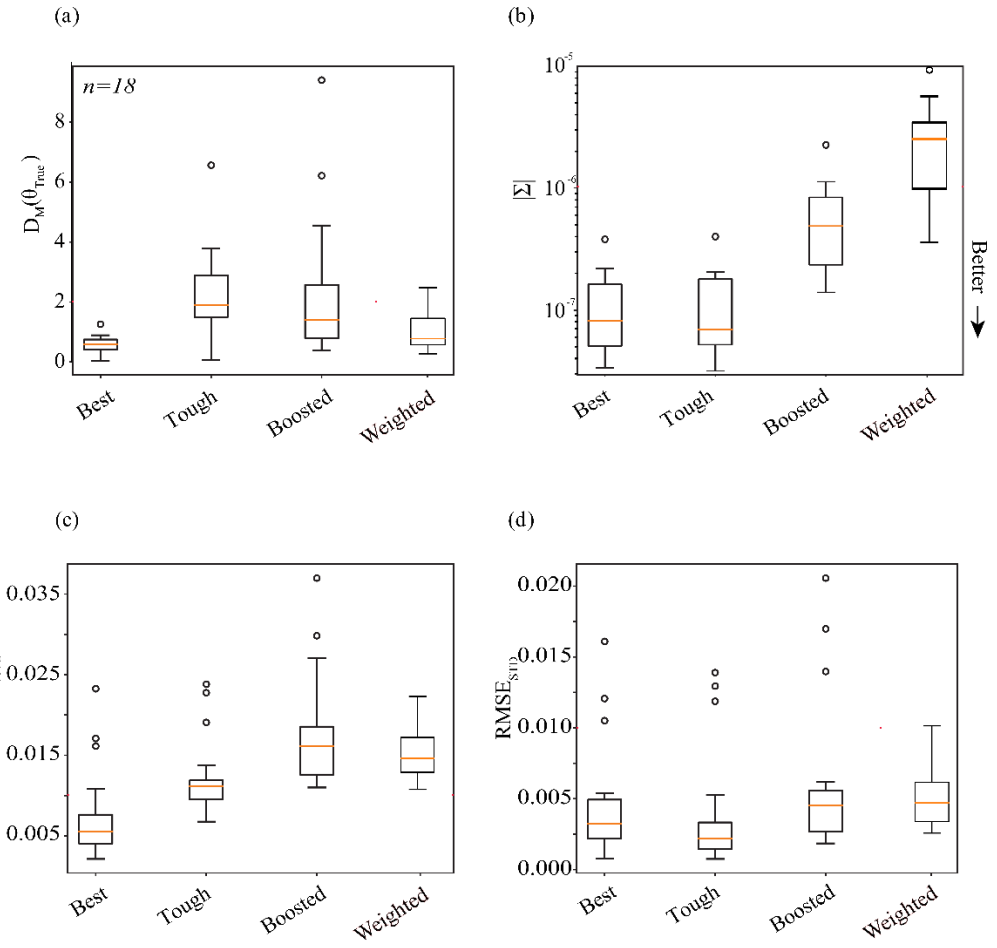


Figure 8: Comparative plots showing the performance of simulation-based inference of parameters and predicted quantities across a set of $n=18$ test data. We compare the results of Experiments 1 ('base' case), 2 ('tough' case), 3 ('boosted' case), and 4 ('weighted' case). Subplots (a) and (b) show the accuracy and precision of parameter inference. Accuracy is shown in subplot (a) via the Mahalanobis Distance of the posterior parameter density. Precision is shown in subplot (b) via the Determinant, $|\Sigma|$. Subplots (c) and (d) show the accuracy and precision of the posterior predictive check. Subplot (c) shows the average of the error, RMSE_{Ave} of streamflow ensembles relative to 'truth', which can be thought of as a measure of accuracy. Subplot (d) shows the standard deviation of the error, RMSE_{std} of streamflow ensembles, which can be thought of as a measure of precision. Values closer to the x-axis are more desirable.

795

800

4.5.2 The precision and accuracy of posterior predictions

Taking this one step further we can use the inferred parameter distributions to generate an ensemble of streamflow simulations using the LSTM and compare this to the observed streamflow (referred to as our posterior predictive check). As shown in Fig. 8C and 8D, the posterior predictions are precise, and generally fairly accurate. Fig. 8C shows the average of the error (RMSE_{Ave}) between the simulated streamflow time series and the observed time series, with lower average error corresponding to greater accuracy. Streamflow prediction accuracy decreases between Experiments 1, 2, and 3. This is represented by the fact that the RMSE_{Ave} increases nearly 3-fold across each of our experiments (median ~ 0.005 in *best case*,

~0.010 in *best case*, and ~0.015 in *boosted case* [scaled streamflow units]). The degradation in posterior predictive accuracy is related to degradation in the accuracy of parameter inference (Figure 8A). Fig. 8D shows the variability of the error 810 (RMSE_{STD}) between the simulated streamflow time series and the observed time series, with lower error variability corresponding to greater precision. We see that the central tendency of the RMSE_{STD} of streamflow simulations for the *base*, *tough*, and *boosted* cases are all similar. Streamflow posterior predictions across all three experiments remained precise, in spite of the breakdown in the accuracy.

In Experiment 4 (the *weighted case*), the posterior predictive accuracy (RMSE_{AVE}) and the average variability 815 (RMSE_{STD}) is improved compared to Experiment 3. Improvement is seen in the outliers, where simulator configurations with a poor fit relative to observed data are assigned low or no weight in Experiment 4 based on the informal likelihood. Importantly, KGE was used in the calculation of the informal likelihood. So, conclusions about the accuracy and precision of posterior predictions associated with the four Experiments may differ as measured by KGE as opposed to RMSE.

The multi-observation comparison helps us to generalize some insights. 1. Inference results are often desirable; in 820 particular, SBI seems to result in precise parameter inference across all conditions. 2. Parameter inference with a well-trained surrogate simulator is precise, but not always suited for conducting inference on observations with an uncertain relationship to simulated data (as in Experiment 2). 3. The performance of posterior predictive checks is dependent on both the performance of the simulator and the neural density estimator. As such it can be a valuable tool in assessing the performance of parameter 825 inference. 4. Although a density estimate derived from an ensemble of simulators (as in Experiment 3) may yield more accurate parameter inference, overconfident parameter estimates are a recalcitrant problem for some observed data. 5. In Experiment 4, an approach to likelihood-weighting parameter estimates from SBI was demonstrated to overcome the problem of overconfidence in these controlled experiments.

5 Discussion

As users of hydrologic tools such as high-fidelity, process-based simulators, we are often interested in finding 830 simulator configuration(s) most consistent with catchment observations and established physical theory. In practice, this gives rise to uncertainty about whether a simulator is “adequate”, as measured by its predictive ability and structural interpretability (Gupta et al, 2012). In the special case where a correct simulator structure exists, the practitioner’s task is to conduct a specification search (Leamer, 1978) to identify it; other candidate simulators inconsistent with observations and theory can be said to be “misspecified” (Cranmer et al., 2020). One example of misspecification in this work is underscored by the misfit 835 between the process based ParFlow and the surrogate LSTM simulators. We call this special situation surrogate misspecification.

Our research shows that using a misspecified surrogate to conduct simulation-based inference for a process-based hydrologic simulator can yield erroneous parameter estimates. These ‘overconfident’ estimates occur because the neural density estimator learns the conditional relationship between parameters and data only from the surrogate simulator. Thus, SBI

840 explicitly infers inputs to the surrogate and *not* parameters of the process-based simulator. Given surrogate misspecification, the inferred values of parameters may not retain their physical significance to the process-based simulator; this can be a barrier to the interpretability of those simulator configurations identified by inference.

845 We demonstrate that erroneous parameter estimates due to surrogate misspecification can be addressed through informal Bayesian model averaging (BMA). This approach to BMA applies a performance check – the informal likelihood – to weight and reject simulator configurations identified by SBI. Notably, the likelihood and related limits of acceptability are chosen by the practitioner based on simulation goals. Thus, broadly, informal BMA belongs to the class of approaches to encode expert / domain knowledge into a deep learning framework (e.g Reichstein et al., 2019). More specifically, SBI 850 conducts a preliminary search of parameter space for plausible simulator structures and configurations, and the likelihood test incorporates expert-defined information about simulator adequacy into the parameter estimates. Overconfident parameter estimates carry the risk of under-representing the uncertainty of the inferences we draw from simulators. Our work shows that, with these two methods in combination, erroneously overconfident parameter estimates are less likely to occur than in standalone SBI.

855 In our experiments we focused investigation on SBI and not the process based simulator. Extending this methodology to observed data requires consideration of many additional sources of uncertainty compared to the synthetic case. Among these is much deeper uncertainty about which simulator structure(s) is (are) appropriate. In the synthetic experiments presented, the relationship between the simulator (the surrogate) and the data-generating process (ParFlow) is well-defined; the surrogate is learned directly from ParFlow. Yet for real hydrologic problems, physics-based simulators are nearly always simplified representations of real data-generating processes; stumbling upon a “true” representation is unlikely, even impossible. Moreover, physical parameters like hydraulic conductivity (K) and Manning’s roughness (M) are themselves conceptual 860 quantities and are almost never known at the scale we care about, making estimates difficult to validate (Oreskes et al., 1994). In this real-world case, the practitioner’s search may be for a set of adequate simulator structures and configurations (i.e. Gupta et. al, 2012), where adequacy is subjectively defined. Here, a reasonably good estimate of the hydrologic variable (i.e., streamflow) is often what catchment scientists strive for (Van Fraassen and others, 1980). For completeness, a worked example demonstrating the estimation of parameters using the current simulator formulation and observed streamflow data from the 865 Taylor catchment is presented in Appendix E. The critic might suggest that not enough was done to tailor the present analysis to real world data. We disagree on the grounds that our purpose here is to rigorously present and evaluate a method for parameter inference given well-defined constraints. The challenge of this goal is real and relevant. In fact, this work seems to show an upper bound for the performance of SBI where undiagnosed structural error exists. A novel simulator averaging approach inspired by Approximate Bayesian Averaging (BMA) and General Likelihood Uncertainty Estimation (GLUE) 870 (Hoeting, 1999; Beven and Binley, 1992) is demonstrated to be an important check to SBI, in presented synthetic and real examples. Further comparison to observations would instead shift the focus of this work from the quality of the SBI and BMA methods to the quality of the underlying hydrologic simulator.

At the core of the challenge of extending SBI is the development of simulators that adequately capture hydrologic behavior. These challenges arise in both the surrogate and the PB simulators. For example, the LSTM surrogate simulator in 875 this study is relatively effective at mimicking ParFlow. This is understandable because the catchment is dominated by snowmelt, which the LSTM mimics well due to its strong memory capabilities. However, in arid catchments, streamflow dynamics are often driven more strongly by short-term reactions to acute rainfall events. LSTMs may struggle to represent these processes (Feng et al, 2020). Additionally, PB simulators are not perfect; for example, Richard's equation may not adequately represent groundwater flow through fractured bedrock (Ofterdinger et al, 2019) or preferential unsaturated zone 880 flow (Vriens et al, 2021). Inadequate surrogate and PB simulator structures may yield erroneous parameter estimates when coupled with SBI.

A more nuanced question regarding simulator adequacy is, "how good is good enough?" For example, when should an LSTM trained on PB simulator representations of arid catchment conditions be used with SBI for parameter estimation? The 885 informal performance weighting approach defines simulator adequacy to exclude poorly performing surrogate simulator structures from the parameter estimation process. Here, the practitioner's "belief" in each simulation defines its adequacy. This performance-weighted approach within the SBI framework can mitigate issues arising from mismatches between the system of interest and the surrogate simulator. If a surrogate trained on arid catchment conditions fails to meet the acceptability criteria, SBI will yield no viable parameter estimates, signaling the need for simulator reevaluation (as explored in Appendix E). This outcome highlights the necessity for practitioners to reconsider the assumed simulator structures, whether surrogate or process 890 based.

The development of robust simulator structures, both surrogates and process-based, remains a central challenge in hydrology. Advances in surrogates capable of representing spatially distributed hydrologic systems, as well as high-fidelity PB simulators, like ParFlow, that capture a broad range of hydrologic processes across various scales, continue to enhance our 895 ability to simulate real hydrologic conditions. As these simulators improve, so too will the overall effectiveness of SBI. Logical next steps to further extend this methodology to the real case are outlined below.

Adding additional complexity to the training set for the surrogate simulator (i.e., exploring a larger number of parameters configurations, their spatial variability, or multiple forcing scenarios) may help yield better estimates and associated predictions. Many of the practitioners of simulation-based inference advocate packing as much complexity into simulators as possible (Alsing and Wandelt, 2019). High-resolution process-based simulators (such as ParFlow) can be used to explore the 900 real-like behaviors of catchments across a great number of variable and parameter configurations by leveraging deep-learned surrogates and SBI. Beyond the informal BMA evaluation of SBI presented here, it may also be important to control for the tradeoff between complexity and parsimony in this expanded set of simulator structures and configurations. This could be achieved using a framework similar to the Akaike Information Criterion (e.g. Schoups et al., 2008), which adds a penalty term related to the number of estimated physical parameters in the likelihood evaluation. A similar 'penalty for complexity' concept 905 was explored in traditional applications of Bayesian Simulator Averaging for statistical models through Occam's Window (Madigan and Raftery, 1994).

SBI is well-suited for inference in high-dimensional space, and has had many adaptations (Cranmer, 2021). As with any approach to inference, scaling to a greater number of parameters will bump into computational constraints. Those constraints come from the cost of simulation (i.e. in the present work, the cost of our PB simulations), and the cost of inference (i.e. the cost of training and evaluating the neural density estimator). In our study, the cost of PB simulation is high, and this has a compounding effect on the cost of inference. Utilizing a surrogate can in some ways reduce the cost of inference, by reducing the need to resort to the more costly PB simulator, but as we show this comes at a tradeoff of accurate parameter estimates if the surrogate is not perfect. Focusing inference on the most informative parts of higher-dimensional parameter space is important if SBI is conducted directly with a costly simulator. Papamakarios' early work with SBI developed sequential neural sampling techniques, which might be less wasteful than other approaches to sampling parameter space (i.e. Papamakarios et al., 2018; Lueckmann et al., 2017; Greenberg et al., 2019). Tsai et al. (2021) use a neural network to learn the mapping between physical parameters and outputs only for PB simulator configurations that correspond closely to observations; SBI can be implemented similarly. However, any framework for parameter learning focused only on observed behaviour needs to be updated as new observations become available and may omit reasonable model configurations from the parameter estimates. Lastly is the option of compressing or reducing the dimensionality, which could be important for the case of estimating distributed parameters. The topic of compression and SBI is explored by Asling, 2019.

Including additional catchment observation types (i.e., groundwater, soil moisture) in the inference workflow could also improve estimates of the physical parameters for real systems, and the predictions associated with complex simulators. However, observations in hydrology – particularly about groundwater systems – are generally sparse. This presents a problem. One option is to observe that complexity *better*. New spatially distributed ‘big data’ products that leverage remote sensing to offer new opportunities to observe hydrologic variables like soil moisture (Mohanty et al., 2017; Petropoulos et al., 2015). The extension of the methodology to real-world observations will also need to consider the role of data quality, adequacy (Gupta et al., 2012), and disinformation (Beven and Westerberg, 2011) and the challenge of defining limits of acceptability regarding model performance.

930 6 Conclusion

Our investigation implements simulation-based inference (SBI) to determine parameters for a spatially distributed, process-based catchment simulator. We believe this research is among the first to apply contemporary SBI to catchment modeling. The implementation employed here has a couple of noteworthy features:

- a. We use deep learning to train a surrogate Long Short-Term Memory (LSTM) on the original physically based simulations (from ParFlow). This allows for quick and comprehensive exploration of simulation results for which we have corresponding observations, such as streamflow at a catchment outflow in a catchment.
- b. A density-based neural network leverages the capacity of the surrogate to generate simulations quickly to learn a representation of the full conditional density, $p(\theta|Y)$, of parameters given data. This learned conditional density can

be evaluated using observations to determine the parameter posterior density, $p(\theta|Y = Y_{Obs})$. This parameter posterior represents our ‘best guess’ of what the parameters for our simulator should be.

940

We demonstrate that this approach to SBI can generate reasonable estimates of the parameters of a hydrologic simulator, ParFlow, through a set of synthetic experiments. We show in Experiment 1 (the *best case*) that SBI works well in controlled settings in which we assume that our surrogate LSTM simulator is accurate. Moreover, this experiment highlights how, once learned, the model of the conditional density can be used to determine the process-based parameters rapidly and effectively for many observations without the need for additional process-based simulations. That’s particularly valuable when simulations are costly, as is often the case with high-resolution, transient simulators used in the field of catchment modeling.

945

We show in Experiment 2 (the *tough case*) that SBI produces a set of probable parameters with precision in settings where the simulator does not represent the underlying system generating the observation perfectly. These inferred parameters are used to generate reasonable streamflow simulations relative to observations. However, the *tough case* shows that parameter inference is not always accurate with respect to the physics-based simulator that was used to train the surrogate. This undesirable characteristic (of precision but not accuracy, or ‘overconfidence’) arises from issues related to the structural adequacy of the simulator, which is well-recognized in the literature as an impediment for accurate parameter inference (Cranmer, 2020). The controlled nature of Experiment 2 explores the special case of ‘surrogate misspecification’. This special case arises from a mismatch between the surrogate and the process-based simulations from ParFlow. In inference, surrogate misspecification gives rise to error in estimates of the physical parameters. We show that sources of this error can be quite difficult to diagnose, although conducting a posterior predictive check is a qualitative way of ascertaining the extent of simulator bias.

950

We show in Experiment 3 (the *boosted case*) that SBI can reduce overconfidence in parameter estimates by using an ensemble of surrogate simulators. In Experiment 4 (the *weighted case*), we show that SBI can incorporate information about the uncertainty of the surrogate simulator to produce more accurate parameter estimates. These experiments demonstrate that SBI can be used to solve the problem of overconfident parameter estimates introduced by surrogate misspecification.

955

In Experiments 3 and 4 (the *boosted* and *weighted cases*, respectively), we attempt to address the issue of ‘overconfident’ parameter inference due to misspecification. In Experiment 3, we use an ensemble of ‘weak’ surrogate simulators (instead of just one ‘strong’ surrogate simulator) to learn the full conditional density. The underlying principle is that the behavior of an ensemble of surrogate simulators *in aggregate* may not be biased, even if each individual simulator has its own bias. This may ‘wash out’ the negative effects of surrogate misspecification on parameter inference. Evidence from the *boosted case* shows this approach reduces the occurrence of overconfident parameter estimates, but is not a silver bullet for conducting accurate inference.

960

In Experiment 4 (the *weighted case*), the practitioner assigns a “measure of belief” to parameter estimates from a set of competing surrogate simulators, reflecting their confidence in its validity. This measure of belief – or informal likelihood (i.e. Beven and Binley, 1992) – is used to weight and reject simulator configurations identified by SBI. The underlying principle is that SBI conducts a preliminary search of parameter space for plausible simulator structures and configurations, and the likelihood test incorporates expert-defined information about simulator adequacy into the parameter estimates. The *weighted case* is demonstrated to solve the problem of overconfident parameter estimates introduced by surrogate misspecification.

970

The results of Experiments 2, 3, and 4 demonstrate progress towards being able to implement SBI in hydrological domains subject to uncertainty we can benchmark (i.e., the misspecification of the surrogate). Additional work is needed to

address deeper uncertainty about the structural adequacy of the underlying physics-based simulator. This uncertainty often exists in catchment modeling – due to (e.g.) natural heterogeneities in the subsurface, approximations in process 975 parameterizations, and bias in the meteorological input data – that can seldom be fully ‘accounted for’. The notion of structural ‘adequacy’ is thus nearly always subjective (Gupta et. al, 2012). In many ‘real world’ applications, a calibrated estimate of the hydrologic variable (i.e., streamflow) is what catchment scientists strive for. Enhancing standalone SBI with the likelihood-weighting methodology introduced in Experiment 4 embraces this principle of subjective ‘adequacy’ and is broadly extendable to more complex inference problems in catchment modeling. Where no simulators are identified as adequate, an obvious next 980 step is to expand the simulator to explore more and different configurations of parameters and input variables.

Appendix A The Process-Based Simulations (ParFlow)

Table A1: The relationship between ParFlow and LSTM static inputs (e.g., parameters, θ), dynamic inputs (e.g., meteorological forcings, X), and dynamic outputs (e.g. streamflow, Y). ParFlow variables must be ‘compressed’ into lower-dimensional representations in order to be used in the LSTM.

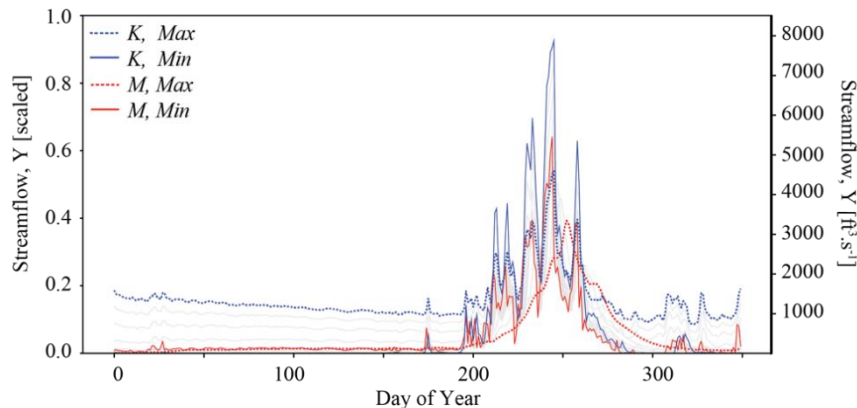
	ParFlow Description	LSTM Description
Parameters, θ	<p>a) 2-dimensional homogeneous Manning’s Roughness, M b) 3-dimensional heterogeneous Hydraulic Conductivity, K</p> <p><i>(Other static inputs, such as soil properties and land cover, are not used by LSTM)</i></p>	<p>a) Scalar value, M_s, set for all values of M b) Scalar factor, K_s, multiplied by all values of K</p> <p><i>(Both are log transformed and re-normalized to be between 0 and 1)</i></p>
Dynamic Outputs, Y	Hourly, 3D spatially distributed pressure field	<p>Daily, 1-dimensional discharge time series (length=350) at i,j location corresponding to USGS gage 09110000, as follows:</p> <ol style="list-style-type: none"> 1. <i>Gridded discharge calculated using surface pressure, slopes, Manning’s, resolution via the overland flow equation for each hourly time step ($n=8,760$) of one year of ParFlow results</i> 2. <i>Slice at i,j location and calculate daily average</i> 3. <i>Remove first 15 days of record (burn in time), and renormalize values between 0 and 1</i>

Dynamic Inputs, X	<p>Hourly, 2D spatially distributed meteorological forcings, including:</p> <ul style="list-style-type: none"> • $DLWR$: Long Wave Radiation [$W.m^{-2}$] • $DSWR$: Short Wave Radiation [$W.m^{-2}$] • $Press$: Atmospheric pressure [pa] • $APCP$: Precipitation [$mm.s^{-1}$] • $Temp$: Air Temperature [K] • $SPFH$: Specific humidity [$kg.kg^{-1}$] • $UGRD$: East-west wind speed [$m.s^{-1}$] • $VGRD$: South-to-North wind speed [$m.s^{-1}$] 	<p>Daily, 1D time series (length=350) for each (n=8) forcing:</p> <p>(Except for $APCP$, forcings are averages taken over space and time for all hours (n=24) in each day. $APCP$ is the sum over space and time for all hours (n=24) of precipitation each day.)</p>
---------------------------------------	--	---

985

Table A2: ParFlow was run many times under different parameter configurations. This table shows the scalar factors used to modify spatially distributed Manning's Coefficient and Hydraulic Conductivity. We call these factors K_s and M_s , respectively, to keep the distinction between them and ParFlow's parameters clear.

	K_s (Scaling factor times whole domain)[unitless]	M_s (Constant across domain), [$h/m^{(1/3)}$]
Scalar Parameters	0.001, 0.01, 0.025, 0.05, 0.075, 0.1, 0.25, 0.5, 0.75, 1, 2.5, 5, 7.5, 10	1e-8, 1e-7, 2.5e-7, 5e-7, 7.5e-7, 1e-6, 2.5e-6, 5e-6, 7.5e-6, 1e-5, 2.5e-5, 5e-5, 1e-4



990

Figure A1: Sensitivity of ParFlow-generated streamflow time series for water year 1995 to perturbations of Hydraulic Conductivity and Mannings. We show sensitivity holding each of K_s and M_s constant at 0.1 and 5×10^{-6} , respectively, while varying the other across the range of parameters explored in Table A2.

Appendix B The Surrogate Simulator (LSTM)

Table B1: Relevant notes on architecture, training, and hyperparameters for the surrogate LSTM simulator.

	LSTM	Further Description
--	------	---------------------

Number of Epochs	300	Number of times iterating through training loops
Batch Size	50	Batching during training
Input Size	10	Number of input features
Hidden Layers	1	Number of hidden layers
Hidden Size	10	Number of hidden nodes / layers
Number of Classes	1	Number of nodes in output
Objective Function	MSE	Mean Squared Error
Optimizer	Adam	
Learning Rate	0.001	
Train-Validation-Test Split	0.7, 0.2, 0.1	Simulations were divided into sets based on their parameters, such that each member characterizes the streamflow response (encoded as a year-long time series) to an individual pair of parameter values K_s and M_s . We conduct the train-validation-test split in a pseudo-Latin hypercube manner across parameters space.

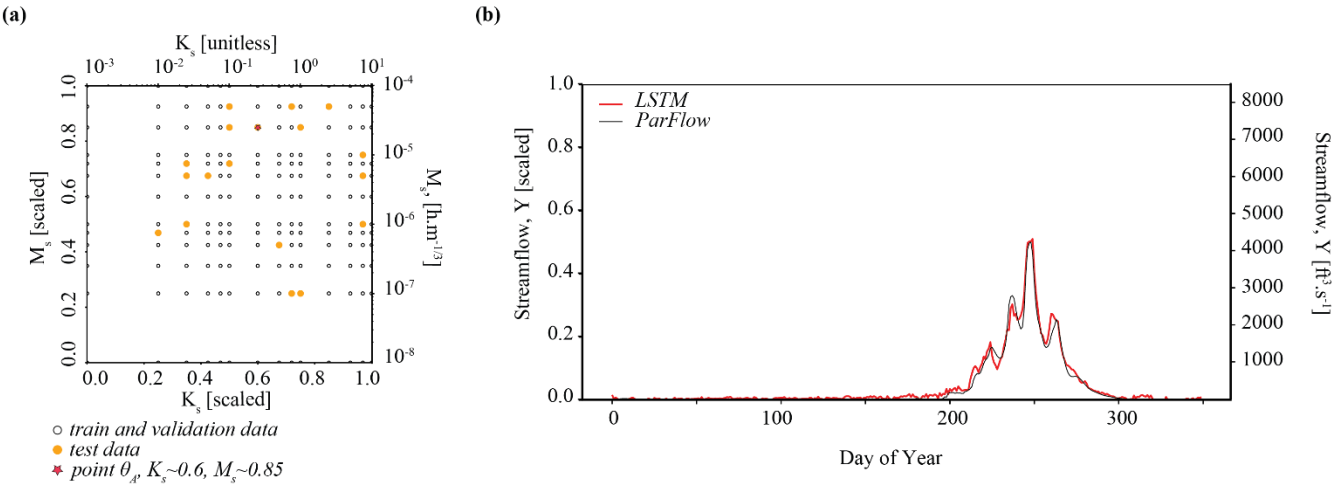


Figure B1: Plots show the train/validation and test split for the LSTM surrogate trained on $n=183$ ParFlow simulations. In (a), the locations in parameter space where ParFlow simulations were run. The surrogate is trained and tested at orange dots. In (b), a comparison of ParFlow to LSTM streamflow simulation generated at benchmark parameter set $\theta_A, K_s \sim 0.6, M_s \sim 0.85$. The fit between ParFlow and LSTM is explored more in the results.

Appendix C Improved Components for SBI

Deriving implicit statistical models using density estimation techniques is not new (Diggle and Gratton, 1984).

However, these traditional approaches suffer from some shortcomings, including sample efficiency and inference quality, as described further in Cranmer, Brehmer, and Louppe 2020. We show two components of the density based SBI workflow utilized here that have benefited due to recent innovations: Masked Autoencoders for Density Estimation (MADEs) and sequential neural posterior sampling.

C.1 Masked Autoencoder for Density Estimation (MADE)

While mixture density networks have a long operational history, there have been more recent innovations in using

neural networks to learn and represent conditional probability distributions. This study utilizes a class of neural density estimators called Masked Autoregressive Flows (Alsing et al., 2019), which shares some of the underlying principles described for Mixture Density Networks. Masked Autoregressive Flows arise from the principle that “any probability density can be factorized as a product of one-dimensional conditionals” via the chain rule (Alsing et al., 2019); these one-dimensional conditionals are parameterized by a fully connected neural network known as a Masked Autoencoder for Density Estimation (MADE) (Uria et al., 2016). Masked Autoregressive Flows are composed of ‘stacks’ of Masked Autoencoder for Density Estimations, to add flexibility (Papamakarios et al., 2018). A detailed description of these methods is beyond the scope of this paper.

C.2 Sequential Neural Posterior Estimation

We use a sampling technique called Sequential Neural Posterior Estimation (SNPE) to speed up and improve the evaluation of a trained neural conditional density estimator. By evaluation, we here mean using data Y (most typically observed data, Y_{Obs}) to generate a posterior estimate $p(\theta | Y = Y_{Obs})$ (step 4 in Sect. 3.5). The need for SNPE arises from the challenge that drawing simulation parameters from the full prior distribution is wasteful (Papamakarios et al., 2018; Lueckmann et al., 2017; Greenberg et al., 2019). This is due to the fact that data simulated from some parts of parameter space have higher or lower posterior density for Y_{Obs} . SNPE iteratively refines the posterior estimate to make inference more efficient and flexible, as described by Greenberg et al, 2019.

Details related to the architectures, hyperparameters, training, and evaluation of neural density estimators are shown in Table C1. Decisions about hyperparameters were made via trial and error. It's important to note that the goal of our work is not to create the most robust neural density estimator model, but to explore inference under a variety of different conditions.

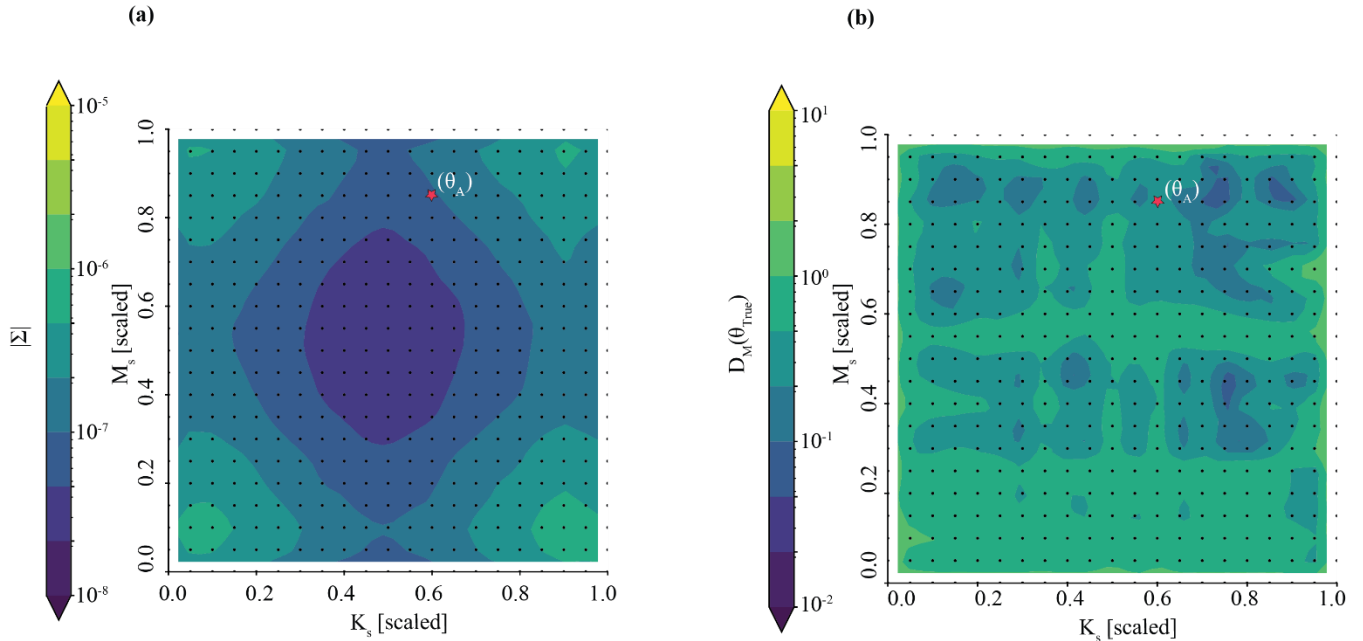
1030 **Table C1: Hyperparameters and model architecture for neural density estimation. See also (Tejero-Cantero et al., 2020).**

Hyper- parameter	Value	Significance
Inference Method	SNPE_C	Sequential Neural Posterior Estimator (see text)
Neural Density Model, $q_\phi(\theta Y)$	MAF	Masked Autoregressive Flow (see text)
Hidden Features	10	number of hidden layers in each MADE of $q_\phi(\theta Y)$
Number of Transforms	2	Number of flows (transforms) between MADEs in $q_\phi(\theta Y)$, MAF
Prior_min, Prior_max	0.0, 1.0	Minimum and Maximum possible values of $q_\phi(\theta Y)$, K_s and M_s
Prior Function	Uniform	All values <i>a priori</i> equally possible in parameter space
Number of simulations	1000	Number of simulated $\{\theta, Y\}$ pairs; used to train $q_\phi(\theta Y)$
Number of samples	5000	Number of sampled $\{\theta, Y\}$ pairs; used to evaluate $q_\phi(\theta Y)$

Appendix D Inference for many observations, $Y_{Obs_LSTM_i}$

A trained neural density estimator can be used to infer the parameters of an observation without the need for additional simulation runs. In this section, we extend Experiment 1 (the ‘best’ case) to evaluate the posterior parameter density for many synthetic observations ($Y_{Obs_LSTM_i}$) quickly and effectively. We use many parameter sets (θ_i) of K_s and M_s sampled uniformly across parameter space to generate an equivalent number of synthetic observations, where $i=1, 2, \dots, 441$.

1035



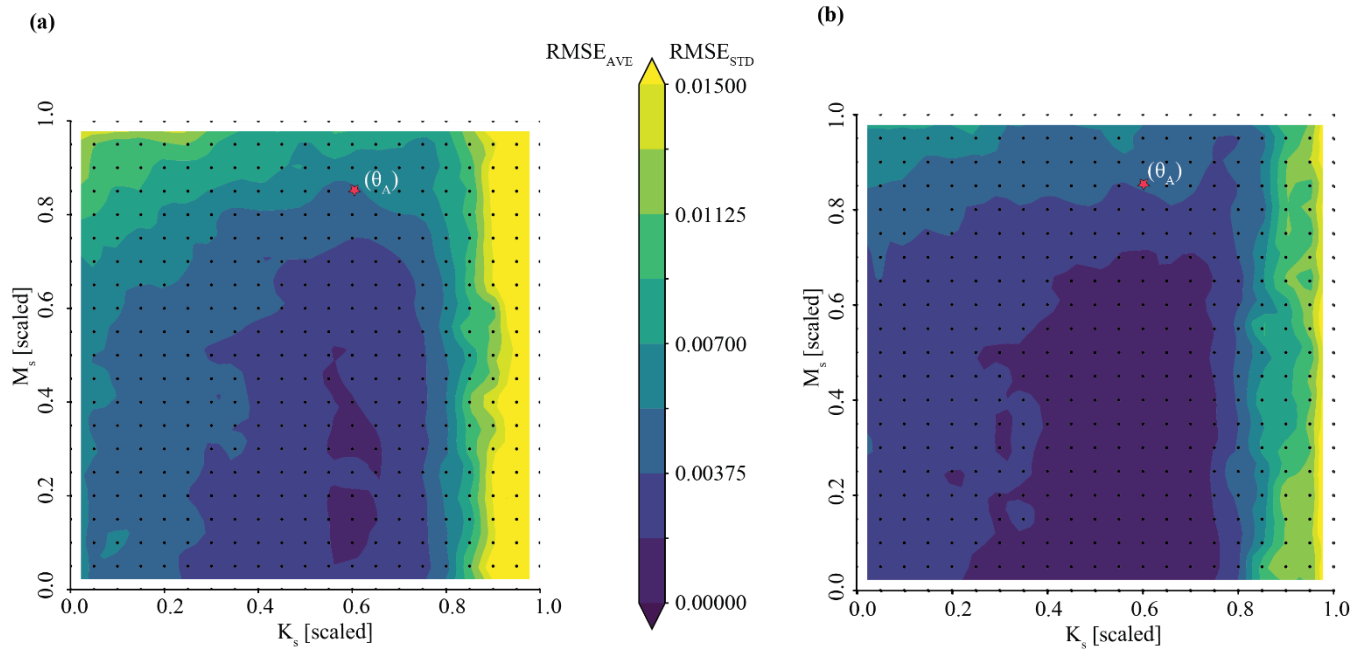
1040 **Figure D1.** Once the neural conditional density estimator is trained, it can be evaluated quickly and effectively given new data. This figure shows the performance of SBI of Mannings (M_s), and Hydraulic Conductivity (K_s) given synthetic streamflow data generated by the surrogate from across 441 locations across parameter space. Subplot (a) shows the Determinant, $|\Sigma|$ of the posterior parameter estimate, which quantifies the precision of parameter inference. Subplot (b) shows the Mahalanobis distance, $D_M(\theta_{True})$ between the inferred distribution and true parameter values, which quantifies the accuracy of inference. These values are shown across the entirety of parameter space investigated, where purple is better. The red star in subplots corresponds with benchmark location θ_A in parameter space of the analysis shown in Figure 3.

1045

SBI can infer the parameters from many diverse and different synthetic observations well, as shown in Figure D1.

The precision of inference of the posterior parameter densities is explored in Figure D1A as a map of determinants across parameter space. Parameter inference is more precise (with a smaller determinant) in the center than at the edges of the 1050 parameter space; it is below our precision threshold of 1×10^{-6} everywhere. Parameter inference is accurate across parameter space, as shown by the map of Mahalanobis Distance in Fig. D1B. There are some pockets of parameter space characterized by more- and less- accurate parameter inference. The structure of the Mahalanobis distances across parameter space doesn’t

1055 seem to be as well-defined as that of the determinant and are likely a consequence of randomness in the initialization of the neural density estimator (confirmed by many independent trials). We note that evaluating each of the synthetic observations in Fig. D1 took only a few seconds.



1060 **Figure D2. Posterior predictive check for many observations:** Once parameters are inferred, the posterior can be drawn (n=50) to generate probabilistic streamflow ensembles. This figure shows the performance of streamflow ensembles derived from SBI at 441 locations across parameter space. Subplot (a) shows the average of the error (RMSE_{ave}) of streamflow ensembles relative to 'truth', which can be thought of as a measure of accuracy. Subplot (b) shows the standard deviation of the error (RMSE_{std}) of streamflow ensembles, which can be thought of as a measure of precision. Streamflow ensembles are evaluated against the 'true' synthetic streamflow time series generated by the surrogate simulator, where blue is better.

1065 The posterior predictive check shows that streamflow characterization is generally both precise and accurate. This required drawing a subset of parameters from *each* of the 441 posterior parameter densities represented as points in Fig. D1 and generating an ensemble of simulated streamflow time series using the surrogate simulator. The accuracy of the posterior predictions is explored in Fig. D2A as a map across parameter space. In general, the posterior predictions have an average error of less than 0.01. Accuracy is highest in the middle of the parameter space and seems to degrade towards the upper 1070 boundaries where parameters K_s and M_s are large. The precision of the posterior predictions is explored in Fig. D2B as a map across parameter space. In general, the posterior predictions are precise, with standard deviation of the error less than 0.01. We note that both the average and standard deviation of error increase at large parameter values, in particular large values of hydraulic conductivity. Overall, Fig. D1 and D2 show that SBI can reliably infer parameters and characterize streamflow processes for *many* streamflow observations that span the parameter space we investigated.

1075

Appendix E Inference on non-synthetic observations at the Taylor River

The informal BMA methodology is suited to assessing the adequacy of model structures and configurations in the real-world case. In Figure E1, inference is conducted on the observed streamflow time series for water year 1995 from the Taylor River gage 09110000 (red). The figure shows the posterior predictive check with confidence intervals from standalone SBI (blue), as well as the “persistence” baseline (orange). Model configurations scoring less than persistence (defined by setting next week’s predicted data equal to today’s observed data) are considered not credible and assigned a weight of zero. Note that standalone SBI does not perform well relative to persistence ($KGE = 0.94$). The culprit is the timing of peak simulated flows, which occur on average some 44 days before the peak observation and 51 days before persistence. With no models superior to persistence, the BMA methodology returns an empty set; no model structures (LSTM surrogates) or configurations (parameter sets) yield predictions that are “reasonably good”. In fact, no model structures or configurations superior to persistence exist in the full space of possible combinations of M and K , as shown by the confidence intervals in grey. We emphasize to the reader that the BMA methodology results in a desirable outcome: all models identified by standalone SBI are rejected, and overconfident predictions and parameter estimates are avoided.

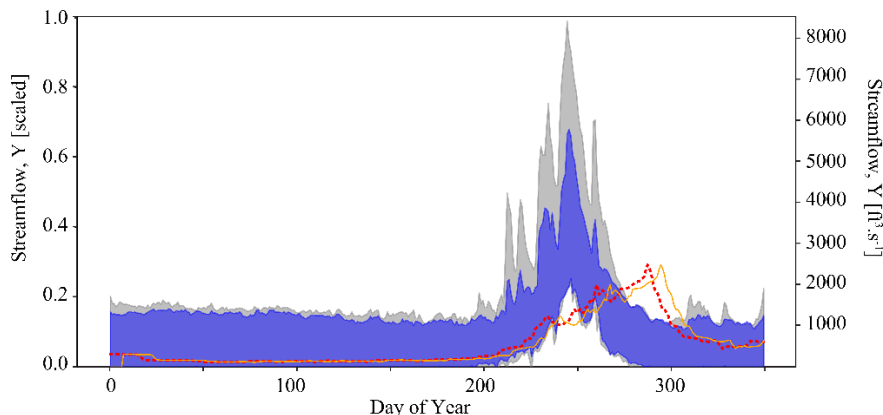


Figure E1. Time series comparing the observed streamflow for water year 1995 (red) with the persistence baseline (orange), posterior predictive check from standalone SBI (blue), and simulations drawn from the full parameter space (gray).

Competing Interests

The contact author has declared that none of the authors has any competing interests

References

Alsing, J. and Wandelt, B. D.: Nuisance hardened data compression for fast likelihood-free inference, Monthly Notices of the Royal Astronomical Society, 2019.

Alsing, J., Charnock, T., Feeney, S., and Wandelt, B.: Fast likelihood-free cosmology with neural density estimators and active learning, *Monthly Notices of the Royal Astronomical Society*, <https://doi.org/10.1093/mnras/stz1960>, 2019.

1100 Bastidas, L., Gupta, H., Sorooshian, S., Shuttleworth, W., and Yang, Z.-L.: Sensitivity analysis of a land surface scheme using multicriteria methods, *Journal of Geophysical Research*, 104, 19481–19490, <https://doi.org/10.1029/1999JD900155>, 1999.

Beven, K. and Binley, A.: The future of distributed models: Model calibration and uncertainty prediction, *Hydrological Processes*, 6, 279–298, <https://doi.org/10.1002/hyp.3360060305>, 1992.

1105 Beven, K.: Rainfall-runoff modelling: the primer, 2012.

Beven, K. and Binley, A.: GLUE: 20 years on, *Hydrological Processes*, 28, 5897–5918, <https://doi.org/10.1002/hyp.10082>, 2014.

1110 Beven, K. and Westerberg, I.: On red herrings and real herrings: disinformation and information in hydrological inference, *Hydrological Processes*, 25, 1676–1680, <https://doi.org/10.1002/hyp.7963>, 2011.

Bishop, C.: *Mixture Density Networks*, 1994.

1115 Castle, S. L., Thomas, B. F., Reager, J. T., Rodell, M., Swenson, S. C., and Famiglietti, J. S.: Groundwater depletion during drought threatens future water security of the Colorado River Catchment, *Geophysical Research Letters*, 41, 5904–5911, <https://doi.org/10.1002/2014GL061055>, 2014.

Condon, L. E.: Scientist Spotlight: Laura Condon, 2022.

Cranmer, K.: A3D3 Seminar: Accelerating Simulation-based Inference | Kyle S. Cranmer, 2022.

Cranmer, K., Brehmer, J., and Louppe, G.: The frontier of simulation-based inference, *Proceedings of the National Academy of Sciences*, 117, 30055–30062, <https://doi.org/10.1073/pnas.1912789117>, 2020.

1120 Diggle, P. J. and Gratton, R. J.: Monte Carlo methods of inference for implicit statistical models, *Journal of the Royal Statistical Society: Series B (Methodological)*, 46, 193–212, 1984.

Draper, D.: Assessment and Propagation of Model Uncertainty, *Journal of the Royal Statistical Society: Series B (Methodological)*, 57, 45–70, <https://doi.org/10.1111/j.2517-6161.1995.tb02015.x>, 1995.

1125 Duan, Q., Ajami, N. K., Gao, X., and Sorooshian, S.: Multi-model ensemble hydrologic prediction using Bayesian model averaging, *Advances in Water Resources*, 30, 1371–1386, <https://doi.org/10.1016/j.advwatres.2006.11.014>, 2007.

Fatichi, S., Vivoni, E. R., Ogden, F. L., Ivanov, V. Y., Mirus, B., Gochis, D., Downer, C. W., Camporese, M., Davison, J. H., Ebel, B., Jones, N., Kim, J., Mascaro, G., Niswonger, R., Restrepo, P., Rigon, R., Shen, C., Sulis, M., and Tarboton, D.: An overview of current applications, challenges, and future trends in distributed process-based models in hydrology, *Journal of Hydrology*, 537, 45–60, <https://doi.org/10.1016/j.jhydrol.2016.03.026>, 2016.

1130 Feng, Dapeng, Kuai Fang, and Chaopeng Shen. “Enhancing Streamflow Forecast and Extracting Insights Using Long-Short Term Memory Networks With Data Integration at Continental Scales.” *Water Resources Research* 56, no. 9 (September 1, 2020): e2019WR026793. <https://doi.org/10.1029/2019WR026793>.

1135 Fenicia, F., Kavetski, D., Reichert, P., and Albert, C.: Signature-Domain Calibration of Hydrological Models Using Approximate Bayesian Computation: Empirical Analysis of Fundamental Properties, *Water Resources Research*, 54, 3958–3987, <https://doi.org/10.1002/2017WR021616>, 2018.

Freund, Y. and Schapire, R. E.: A Decision-Theoretic Generalization of On-Line Learning and an Application to Boosting, *Journal of Computer and System Sciences*, 55, 119–139, <https://doi.org/10.1006/jcss.1997.1504>, 1997.

Gabry, J., Simpson, D., Vehtari, A., Betancourt, M., and Gelman, A.: Visualization in Bayesian workflow, *Journal of the Royal Statistical Society: Series A (Statistics in Society)*, 182, 389–402, <https://doi.org/10.1111/rssa.12378>, 2019.

1140 Greenberg, D. S., Nonnenmacher, M., and Macke, J. H.: Automatic Posterior Transformation for Likelihood-Free Inference, , <https://doi.org/10.48550/ARXIV.1905.07488>, 2019.

Gupta, H. V., Sorooshian, S., and Yapo, P. O.: Toward improved calibration of hydrologic models: Multiple and noncommensurable measures of information, *Water Resources Research*, 34, 751–763, <https://doi.org/10.1029/97WR03495>, 1998.

1145 Gupta, H. V., Kling, H., Yilmaz, K. K., and Martinez, G. F.: Decomposition of the mean squared error and NSE performance criteria: Implications for improving hydrological modelling, *Journal of Hydrology*, 377, 80–91, <https://doi.org/10.1016/j.jhydrol.2009.08.003>, 2009.

Gupta, H. V., Clark, M. P., Vrugt, J. A., Abramowitz, G., and Ye, M.: Towards a comprehensive assessment of model 1150 structural adequacy, *Water Resources Research*, 48, <https://doi.org/10.1029/2011WR011044>, 2012.

Hermans, J., Delaunoy, A., Rozet, F., Wehenkel, A., and Louppe, G.: A Crisis In Simulation-Based Inference? Beware, Your Posterior Approximations Can Be Unfaithful, *Transactions on Machine Learning Research*, 2022.

Hochreiter, S. and Schmidhuber, J.: Long Short-Term Memory, *Neural computation*, 1735–1780, 1155 <https://doi.org/10.1162/neco.1997.9.8.1735>, 1997.

Jennifer A. Hoeting, David Madigan, Adrian E. Raftery, and Chris T. Volinsky: Bayesian model averaging: a tutorial (with comments by M. Clyde, David Draper and E. I. George, and a rejoinder by the authors, *Statistical Science*, 14, 382–417, <https://doi.org/10.1214/ss/1009212519>, 1999.

1160 Hunt, R. J., Doherty, J., and Tonkin, M. J.: Are Models Too Simple? Arguments for Increased Parameterization, *Groundwater*, 45, 254–262, <https://doi.org/10.1111/j.1745-6584.2007.00316.x>, 2007.

Jiang, S., Zheng, Y., and Solomatine, D.: Improving AI system awareness of geoscience knowledge: Symbiotic integration of physical approaches and deep learning, *Geophysical Research Letters*, 47, e2020GL088229, 2020.

Jones, J. E. and Woodward, C. S.: Newton-Krylov-multigrid solvers for large-scale, highly heterogenous, variably saturated 1165 flow problems, *Advances in Water Resources*, 763–774, [https://doi.org/10.1016/S0309-1708\(00\)00075-0](https://doi.org/10.1016/S0309-1708(00)00075-0), 2001.

Karpatne, A., Atluri, G., Faghmous, J. H., Steinbach, M., Banerjee, A., Ganguly, A., Shekhar, S., Samatova, N., and Kumar, V.: Theory-guided data science: A new paradigm for scientific discovery from data, *IEEE Transactions on knowledge and data engineering*, 29, 2318–2331, 2017.

Kollet, S. J. and Maxwell, R. M.: Capturing the influence of groundwater dynamics on land surface processes using an 1170 integrated, distributed catchment model, *Water Resources Research*, <https://doi.org/10.1029/2007wr006004>, 2008.

Kratzert, F., Klotz, D., Brenner, C., Schulz, K., and Herrnegger, M.: Rainfall–runoff modelling using Long Short-Term Memory (LSTM) networks, *Hydrology and Earth System Sciences*, 22, 6005–6022, <https://doi.org/10.5194/hess-22-6005-2018>, 2018.

1175 Leonarduzzi, E., Tran, H., Bansal, V., Hull, R. B., De la Fuente, L., Bearup, L. A., Melchior, P., Condon, L. E., and Maxwell, R. M.: Combining Machine learning and Physics-based hydrological Modeling to predict 2D soil moisture fields in a changing climate, *Frontiers*, Publication Forthcoming, 2022.

Leamer, E. E.: *Specification searches : ad hoc inference with nonexperimental data*, Wiley, 1978.

Lueckmann, J.-M., Goncalves, P. J., Bassetto, G., Öcal, K., Nonnenmacher, M., and Macke, J. H.: Flexible statistical inference for mechanistic models of neural dynamics, , <https://doi.org/10.48550/ARXIV.1711.01861>, 2017.

1180 Madigan, D. and Raftery, A. E.: Model Selection and Accounting for Model Uncertainty in Graphical Models Using Occam’s Window, *Journal of the American Statistical Association*, 89, 1535–1546, <https://doi.org/10.1080/01621459.1994.10476894>, 1994.

Maesschalck, R. D., Jouan-Rimbaud, D., and Massart, D. L.: The Mahalanobis distance, *Chemometrics and Intelligent Laboratory Systems*, 50, 1–18, [https://doi.org/10.1016/S0169-7439\(99\)00047-7](https://doi.org/10.1016/S0169-7439(99)00047-7), 2000.

1185 4.3 Determinants and Volumes: <https://textbooks.math.gatech.edu/ila/determinants-volumes.html>.

Maxwell, R. M. and Kollet, S. J.: Integrated surface–groundwater flow modeling: A free-surface overland flow boundary condition in a parallel groundwater flow model, *Advances in Water Resources*, 945–958, <https://doi.org/10.1016/j.advwatres.2005.08.006>, 2006.

1190 Maxwell, R. M. and Miller, N. L.: Development of a Coupled Land Surface and Groundwater Model, *Journal of Hydrometeorology*, 233–247, <https://doi.org/10.1175/JHM422.1>, 2005.

Maxwell, R. M., Condon, L. E., and Kollet, S. J.: A high-resolution simulation of groundwater and surface water over most of the continental US with the integrated hydrologic model ParFlow v3, *Geoscientific Model Development*, 8, 923–937, <https://doi.org/10.5194/gmd-8-923-2015>, 2015a.

1195 Maxwell, R. M., Condon, L. E., and Kollet, S. J.: A high-resolution simulation of groundwater and surface water over most of the continental US with the integrated hydrologic model ParFlow v3, *Geoscientific Model Development*, 923–937, <https://doi.org/10.5194/gmd-8-923-2015>, 2015b.

Maxwell, R. M., Condon, L. E., and Melchior, P.: A Physics-Informed, Machine Learning Emulator of a 2D Surface Water Model: What Temporal Networks and Simulation-Based Inference Can Help Us Learn about Hydrologic Processes, *Water*, 13, <https://doi.org/10.3390/w13243633>, 2021.

1200 Mohanty, B. P., Cosh, M. H., Lakshmi, V., and Montzka, C.: Soil moisture remote sensing: State-of-the-science, *Vadose Zone Journal*, 16, 1–9, 2017.

Nearing, G. S., Tian, Y., Gupta, H. V., Clark, M. P., Harrison, K. W., and Weijs, S. V.: A philosophical basis for hydrological uncertainty, *Hydrological Sciences Journal*, 61, 1666–1678, <https://doi.org/10.1080/02626667.2016.1183009>, 2016.

1205 Ofterdinger, U., A. M. MacDonald, J.-C. Comte, and M. E. Young. “Groundwater in Fractured Bedrock Environments: Managing Catchment and Subsurface Resources – an Introduction.” In *Groundwater in Fractured Bedrock Environments*:

Managing Catchment and Subsurface Resources, edited by U. Oftedinger, A.M. MacDonald, J.-C. Comte, and M.E. Young, 479:0. Geological Society of London, 2019. <https://doi.org/10.1144/SP479-2018-170>.

Oreskes, N., Shrader-Frechette, K., and Belitz, K.: Verification, Validation, and Confirmation of Numerical Models in the Earth Science, *Science* (New York, N.Y.), 263, 641–6, <https://doi.org/10.1126/science.263.5147.641>, 1994.

1210 Paniconi, C. and Putti, M.: Physically based modeling in catchment hydrology at 50: Survey and outlook, *Water Resources Research*, 51, 7090–7129, <https://doi.org/10.1002/2015WR017780>, 2015.

Papamakarios, G. and Murray, I.: Fast \mathcal{E} -free Inference of Simulation Models with Bayesian Conditional Density Estimation, , <https://doi.org/10.48550/ARXIV.1605.06376>, 2016.

1215 Papamakarios, G., Sterratt, D. C., and Murray, I.: Sequential Neural Likelihood: Fast Likelihood-free Inference with Autoregressive Flows, , <https://doi.org/10.48550/ARXIV.1805.07226>, 2018.

Petropoulos, G. P., Ireland, G., and Barrett, B.: Surface soil moisture retrievals from remote sensing: Current status, products & future trends, *Physics and Chemistry of the Earth, Parts A/B/C*, 83, 36–56, 2015.

Raftery, A. E., Gneiting, T., Balabdaoui, F., and Polakowski, M.: Using Bayesian Model Averaging to Calibrate Forecast Ensembles, *Monthly Weather Review*, 133, 1155–1174, <https://doi.org/10.1175/MWR2906.1>, 2005.

1220 Reichstein, M., Camps-Valls, G., Stevens, B., Jung, M., Denzler, J., Carvalhais, N., and Prabhat: Deep learning and process understanding for data-driven Earth system science, *Nature*, 566, 195–204, <https://doi.org/10.1038/s41586-019-0912-1>, 2019.

Rumelhart, D. E., Hinton, G. E., and Williams, R. J.: Learning representations by back-propagating errors, *Nature*, 323, 533–536, <https://doi.org/10.1038/323533a0>, 1986.

1225 Santos, N. and Patno, H.: Operations Plan for Colorado River Reservoirs, Bureau of Reclamation, 2022.

Schoups, G., van de Giesen, N. C., and Savenije, H. H. G.: Model complexity control for hydrologic prediction, *Water Resources Research*, 44, <https://doi.org/10.1029/2008WR006836>, 2008.

1230 Smith, P., Beven, K. J., and Tawn, J. A.: Informal likelihood measures in model assessment: Theoretic development and investigation, *Advances in Water Resources*, 31, 1087–1100, <https://doi.org/10.1016/j.advwatres.2008.04.012>, 2008.

Tejero-Cantero, A., Boelts, J., Deistler, M., Lueckmann, J.-M., Durkan, C., Gonçalves, P. J., Greenberg, D. S., and Macke, J. H.: sbi: A toolkit for simulation-based inference, *Journal of Open Source Software*, 5, 2505, <https://doi.org/10.21105/joss.02505>, 2020.

Tenney, W.: A Tier 2a Shortage is confirmed, but uncertainty remains, Arizona Municipal Water Users Association, 2022.

1235 Tran, H., Leonarduzzi, E., De la Fuente, L., Hull, R. B., Bansal, V., Chennault, C., Gentile, P., Melchior, P., Condon, L. E., and Maxwell, R. M.: Development of a Deep Learning Emulator for a Distributed Groundwater–Surface Water Model: ParFlow-ML, *Water*, 13, <https://doi.org/10.3390/w13233393>, 2021.

Tran, H., Zhang, J., O'Neill, M. M., Ryken, A., Condon, L. E., and Maxwell, R. M.: A hydrological simulation dataset of the Upper Colorado River Catchment from 1983 to 2019, *Scientific Data*, 9, 16, <https://doi.org/10.1038/s41597-022-01123-w>, 2022.

Tsai, W.-P., Feng, D., Pan, M., Beck, H., Lawson, K., Yang, Y., Liu, J., and Shen, C.: From calibration to parameter learning: Harnessing the scaling effects of big data in geoscientific modeling, *Nature Communications*, 12, 5988, <https://doi.org/10.1038/s41467-021-26107-z>, 2021.

1245 Uria, B., Côté, M.-A., Gregor, K., Murray, I., and Larochelle, H.: Neural Autoregressive Distribution Estimation, *Journal of Machine Learning Research*, 17, 1–37, 2016.

Van Fraassen, B. C. and others: *The scientific image*, Oxford University Press, 1980.

Vriens, Bas, Benoît Plante, Nicolas Seigneur, and Heather Jamieson. “Mine Waste Rock: Insights for Sustainable Hydrogeochemical Management.” *Minerals* 10, no. 9 (August 19, 2020): 728. <https://doi.org/10.3390/min10090728>.

1250 Vrugt, J. A. and Sadegh, M.: Toward diagnostic model calibration and evaluation: Approximate Bayesian computation, *Water Resources Research*, 49, 4335–4345, <https://doi.org/10.1002/wrcr.20354>, 2013.

Weiss, G. and von Haeseler, A.: Inference of Population History Using a Likelihood Approach, *Genetics*, 149, 1539–46, <https://doi.org/10.1093/genetics/149.3.1539>, 1998.

1255 White, J. T., Hunt, R. J., Fienen, M. N., and Doherty, J. E.: Approaches to highly parameterized inversion: PEST++ Version 5, a software suite for parameter estimation, uncertainty analysis, management optimization and sensitivity analysis, Reston, VA, <https://doi.org/10.3133/tm7C26>, 2020.

Wikle, C. K. and Berliner, L. M.: A Bayesian tutorial for data assimilation, *Physica D: Nonlinear Phenomena*, 230, 1–16, <https://doi.org/10.1016/j.physd.2006.09.017>, 2007.

1260 Wilkinson, M. D., Dumontier, M., Aalbersberg, I. J. J., Appleton, G., Axton, M., Baak, A., Blomberg, N., Boiten, J.-W., da Silva Santos, L. B., Bourne, P. E., Bouwman, J., Brookes, A. J., Clark, T., Crosas, M., Dillo, I., Dumon, O., Edmunds, S., Evelo, C. T., Finkers, R., Gonzalez-Beltran, A., Gray, A. J. G., Groth, P., Goble, C., Grethe, J. S., Heringa, J., 't Hoen, P. A. C., Hooft, R., Kuhn, T., Kok, R., Kok, J., Lusher, S. J., Martone, M. E., Mons, A., Packer, A. L., Persson, B., Rocca-Serra, P., Roos, M., van Schaik, R., Sansone, S.-A., Schultes, E., Sengstag, T., Slater, T., Strawn, G., Swertz, M. A., Thompson, M., van der Lei, J., van Mulligen, E., Velterop, J., Waagmeester, A., Wittenburg, P., Wolstencroft, K., Zhao, J., and Mons, B.: The FAIR Guiding Principles for scientific data management and stewardship., *Sci Data*, 3, 160018, <https://doi.org/10.1038/sdata.2016.18>, 2016.

1265 Williams, A. P., Cook, B. I., and Smerdon, J. E.: Rapid intensification of the emerging southwestern North American megadrought in 2020–2021, *Nature Climate Change*, 12, 232–234, <https://doi.org/10.1038/s41558-022-01290-z>, 2022.

Zhao, W. L., Gentine, P., Reichstein, M., Zhang, Y., Zhou, S., Wen, Y., Lin, C., Li, X., and Qiu, G. Y.: Physics-constrained machine learning of evapotranspiration, *Geophysical Research Letters*, 46, 14496–14507, 2019.

1270